Technical Report

TR-11-07

Report on hydro-mechanical and chemical-mineralogical analyses of the bentonite buffer in Canister Retrieval Test

Ann Dueck, Lars-Erik Johannesson
Ola Kristensson, Siv Olsson

Clay Technology AB

December 2011

Svensk Kärnbränslehantering AB
Swedish Nuclear Fuel
and Waste Management Co

Box 250, SE-101 24 Stockholm
Phone +46 8 459 84 00

ISSN 1404-0344
SKB TR-11-07

Report on hydro-mechanical and chemical-mineralogical analyses of the bentonite buffer in Canister Retrieval Test

Ann Dueck, Lars-Erik Johannesson
Ola Kristensson, Siv Olsson

Clay Technology AB

December 2011

Keywords: Bentonite, Crystal chemistry, Field experiment, Hydraulic conductivity, Hydrothermal, Montmorillonite, Swelling pressure, Unconfined compression test.

Abstract

The effect of five years of exposure to repository-like conditions on compacted Wyoming bentonite was determined by comparing the hydraulic, mechanical, and mineralogical properties of samples from the bentonite buffer of the Canister Retrieval Test (CRT) with those of reference material. The CRT, located at the Swedish Äspö Hard Rock Laboratory (HRL), was a full-scale field experiment simulating conditions relevant for the Swedish KBS-3 concept for disposal of high-level radioactive waste in crystalline host rock. The compacted bentonite, surrounding a copper canister equipped with heaters, had been subjected to heating at temperatures up to 95°C and hydration by natural Na-Ca-Cl type groundwater for almost five years at the time of retrieval.

Under the thermal and hydration gradients that prevailed during the test, sulfate in the bentonite was redistributed and accumulated as anhydrite close to the canister. The major change in the exchangeable cation pool was a loss in Mg in the outer parts of the blocks, suggesting replacement of Mg mainly by Ca along with the hydration with groundwater. Close to the copper canister, small amounts of Cu were incorporated in the bentonite. A reduction of strain at failure was observed in the innermost part of the bentonite buffer, but no influence was seen on the shear strength. No change of the swelling pressure was observed, while a modest decrease in hydraulic conductivity was found for the samples with the highest densities. No coupling was found between these changes in the hydro-mechanical properties and the montmorillonite – the X-ray diffraction characteristics, the cation exchange properties, and the average crystal chemistry of the Na-converted < 1 μm fractions provided no evidence of any chemical/structural changes in the montmorillonite after the 5-year hydrothermal test.

Sammanfattning

Wyoming-bentonit som under cirka fem år exponerats för förhållanden liknande dem som förväntas i ett KBS-3 förvar för använt kärnbränsle i urberg har undersökts med avseende på förändringar hos hydrauliska, mekaniska och kemiska/minerarologiska egenskaper. Studierna baserades på jämförelser av oexponerad referensbentonit och prov tagna på bentonitbufferten i försöket Prov av Återtag vid Äspö-laboratoriet. Försöket var ett fullskaligt fältexperiment, som avsåg att simulera de förhållanden som kommer att råda i ett KBS-3 förvar. Bufferten bestod av kompakterade block och pellets av MX-80 bentonit, som omgav en kopparkapsel, försedd med elektriska värmare. Vid provtagningen hade bufferten under knappt fem år utsatts för förhöjda temperaturer (upp till ~ 95° C) och bevätning med det naturliga Na-Ca-Cl-dominerade grundvattnet från omkringliggande berg.

Under de termiska gradienter och bevätningsförhållanden som rådde under experimentet omfördelades kalciumsulfat i bentoniten, vilket ledde till förhöjda sulfathalter i form av anhydrit i bentoniten närmast kapseln. En viss minskning av utbytbart magnesium hade skett i de yttre delarna av blocken, där magnesium ersatts huvudsakligen av kalcium på grund av bevätningen med grundvatten. Intill kopparkapseln var Cu-halten i bentoniten något förhöjd. För material från de inre delarna av bufferten hade töjningen vid brott minskat något, medan skjuvspänningen vid brott var oförändrad. Svälltrycket var oförändrat och en liten minskning av den hydrauliska konduktiviteten uppmättes för proverna med hög densitet. Någon koppling mellan förändringarna i de hydro-mekaniska egenskaperna och montmorilloniten kunde inte påvisas – varken röntgendiffraktionsegenskaperna, katjonsbyteskapaciteten, eller kristallstrukturen hos Na-konverterade < 1 μm fraktioner gav några indikationer på kemiska/strukturella förändringar hos montmorilloniten efter det femåriga experimentet.

Contents

1 Introduction

This report presents the results of hydro-mechanical and chemical-mineralogical analyses of the excavated bentonite buffer from the Canister Retrieval Test (CRT) field experiment. The effects of repository-like conditions on the bentonite were investigated by comparing the properties of the exposed bentonite with those of reference material.

The following tests/analyses were performed:

- Bentonite composition
- Aqueous leachates
- Exchangeable cations and cation exchange capacity (CEC)
- X-ray diffraction analysis
- Swelling pressure
- Hydraulic conductivity
- Unconfined compression test

The chemical-mineralogical and hydro-mechanical analyses are presented in Chapter 3 and 4, respectively.

1.1 Background

According to the Swedish KBS-3 concept, designed by the Swedish Nuclear and Waste Management Co. (SKB) for disposal of high-level radioactive waste, the spent fuel will be stored in copper canisters embedded in bentonite buffer in vertical emplacement boreholes at a depth of ~500 m in crystalline bedrock. The primary and secondary sets of safety functions of the buffer (SKB 2011) are related to containment of the fuel within the canister and retardation of a potential release of radio nuclides from the repository, respectively. A buffer of highly compacted bentonite is considered a good choice to fullfill these saftety functions due to its favourable hydro-mechanical and chemical properties, such as low hydraulic conductivity, good swelling ability, and plasticity. All these properties of the bentonite are directly related to the crystal chemistry of the predominant mineral smectite. Therefore, the stability of the smectite when subjected to elevated temperatures and hydration from the host rock is of vital importance for the long-term performance of the buffer.

Quantitatively, the most important temperature dependent reaction in bentonites is the progressive conversion of smectite to illite, which has been extensively studied because of its relevance as geothermometer in explorations for hydrocarbons. Besides a large number of studies on illitization in different geological settings (review in Weaver 1989), numerous hydrothermal laboratory experiments have been made but there is still no general consensus on whether the conversion of smectite to illite is primarily controlled by pressure, temperature, potassium activity, pH, silica activity, or other factors. (e.g. Abercrombie et al. 1994, Eberl et al. 1993, Hower et al. 1976, Weaver 1989). The design criteria for the KBS-3 repository stipulate that the temperature should never exceed 100°C at any position in the buffer. Karnland and Birgersson (2006) estimated the smectite-to-illite conversion under these conditions to be insignificant, using the kinetic model and constants of Huang et al. (1993) and extreme values of the potassium concentration in the groundwater at the Äspö HRL.

During the past decades a growing number of laboratory and field tests at different scales, of different design and of durations from months to a couple of years have been performed in order to study the effects of simulated repository-like conditions on bentonite clays. These experiments have highlighted mainly thermo-hydraulic processes, water and solute transports and geochemical reactions under the transient thermal and hydration gradients prevalent during the initial stage of the operation of a repository (Karnland et al. 2000, Dixon et al. 2002, Huertas et al. 2006, Plötze et al. 2007, Villar and Lloret 2007, Gens et al. 2009, Karnland et al. 2009, Fernández and Villar 2010, Gómez-Espina and Villar 2010).

The CRT experiment was a 5 year-long, full-scale field test, designed according to the KBS-3 specifications. Heaters were installed in the canister to simulate the thermal activity of the waste, and filters were installed at the walls of the deposition hole to control the water saturation process in the buffer. The experiment was installed at Äspö Hard Rock Laboratory, Sweden, managed by SKB.

The primary objectives of the CRT experiment were to demonstrate the technique for retrieving emplaced canisters with the bentonite buffer completely water saturated (Eng 2008), and also to monitor thermal, hydraulic, and mechanical processes in the bentonite during the operational phase (Goudarzi et al. 2006). The retrieving technique was, however, tested only on the lower half of the buffer which made it possible to sample the upper half of the buffer for determinations of the bentonite properties after the hydrothermal exposure.

The state of the buffer in terms of basic geotechnical properties, such as water content and dry density, was determined in connection with the retrieval and are reported by Johannesson (2007). The present report addresses potential effects on the bentonite of the exposure to conditions similar to those expected during the initial operational stage of a KBS-3 repository. This report is the complete compilation of the test results, however, a large part of the results was published by Dueck et al. (2011).

2 Description of the CRT field experiment

The CRT experiment was located in the main test area at the –420 m level in Äspö HRL. A schematic overview of the experiment is shown in Figure 2-1. The CRT experiment was a full scale experiment similar to the so called KBS-3 concept and as such performed in crystalline host rock. A full-size copper canister was equipped with heaters to simulate the thermal activity of the high level waste. As can be seen in Figure 2-1, there was no tunnel backfill in the setup. In the experiment, the mechanical reaction of the tunnel backfill was simulated by use of a vertically mobile concrete plug, whose motion was restrained by the elasticity in nine rock anchors connected to a steel lid placed on top of the plug.

In order to control the wetting process and increase the saturation rate, filters connected to groundwater taken from an adjacent bore hole were installed at the borehole wall. The filters, fixed to the rock wall in a pattern shown in Figure 2-2, were made of four layers of strips of a porous plastic filter material. 16 strips with the width 10 cm and length 6.25 m were applied with equal individual distance. The filters did not cover the entire deposition hole surface in order for the bentonite to be able to seal against the plug and also to avoid issues with the slits in the rock. The filter strips also made the water supply approximately homogeneous, which is of great convenience when analyzing the experiment

The buffer surrounding the canister consisted of compacted Wyoming bentonite with the brand name Volclay MX-80, a sodium-dominated bentonite produced by American Colloid Company. Ten ring-shaped blocks (labeled R1 to R10 from bottom to top) surrounded the canister and cylinder-shaped bentonite blocks were placed below (C1) and above (C2 to C4) the canister. The positions and dimensions of the cylindrical and ring-shaped blocks are given in Figure 2-1. The empty volume inside block R10, between the bottom of block C2 and the canister, was filled with brick-shaped bentonite blocks. The slot between the buffer blocks and the borehole wall was filled with bentonite pellets.

The timeline of the experiment may be divided in three subsequent phases: Installation, Operation, and Excavation. The activities during each of the phases are described in the following sections together with data that are relevant for the present study.

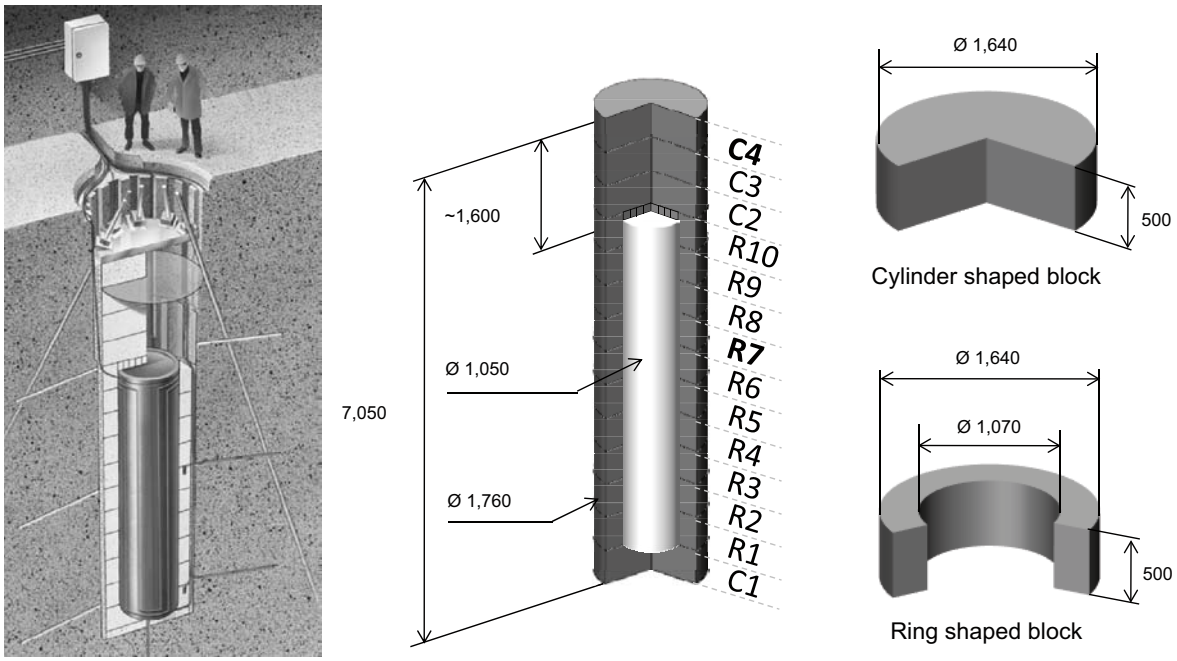

Figure 2-1. *A schematic overview of CRT (left) and dimensions (mm) of the buffer in the deposition hole (right).*

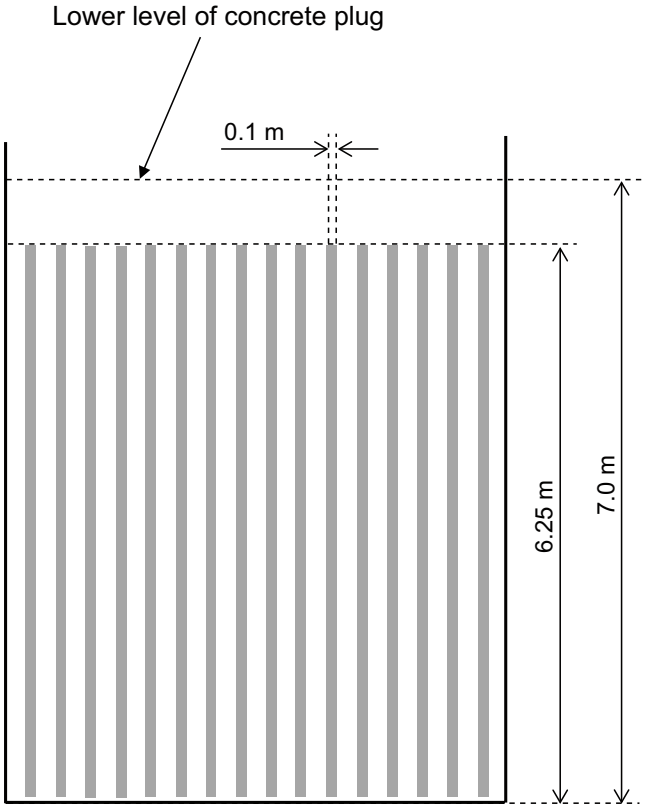

Figure 2-2. *Schematic drawing of the location of filter strips in the wetting system.*

2.1 Installation phase

The installation phase started in 1999 with the drilling of the deposition hole, casting of the concrete foundation, and installation of the artificial water supply (filters fitted at the borehole wall). Installation of bentonite blocks, of which five were instrumented (C4, C3, R10, R5 and C1), and the heater-equipped canister followed. The filling of the slot between the buffer blocks and the hole wall with bentonite pellets and water is considered the end of the installation phase since after this point, HM-processes in the buffer were initiated. The installation procedure is described in detail in Thorsager et al. (2002).

In Table 2-1 the initial conditions of the buffer are given in terms of basic geotechnical properties determined as described in Appendix 2. Two different states are specified for the pellet-filled slot, before (Pellets I) and after (Pellets II) the voids between the pellets were filled with water.

Table 2-1 Estimated values of density, water content, void ratio, and degree of saturation for different parts of the buffer before the saturation phase.

Section	Density (kg/m^3)	Water content	Dry density (kg/m^3)	Void ratio	Degr. of saturation
Cylinder-shaped block	1,991	0.172	1,699	0.636	0.751
Ring-shaped block	2,087	0.171	1,782	0.560	0.849
Brick-shaped block	1,883	0.165	1,616	0.720	0.637
Pellet slot I	1,101	0.100	1,001	1.778	0.156
Pellet slot II	1,574	0.572	1,001	1.778	0.895

2.2 Operational phase

The operational phase started in October 2000 with the casting of the vertically mobile concrete plug on top of the buffer. This was followed by placement of the steel lid on top of the plug and anchoring the lid to the rock by the nine steel wires, shown in Figure 2-1. After this the heater power and the water pressure in the filters were set according to the protocols and the evolutions of thermal, hydraulic and mechanical variables were monitored. The sensor data collected during the operational phase is reported in Goudarzi et al. (2006).

When the buffer was retrieved in 2006 the bentonite had been subjected to hydration by a Na-Ca-Cl-dominated groundwater (Table 2-2) and elevated temperature for almost 5 years during the operational phase. The recorded temperature evolution (Figure 2-3, left) in the buffer at canister mid-height (ring 5) and at the top of the buffer-filled volume (cylinder 4) shows that steady state heat flow conditions were reached during the first year of the experiment. For approximately 3 years the temperature at the radius 585 mm was 75–87°C and a radial thermal gradient of ~1°C/cm prevailed. Figure 2-3 (right) shows conditions at ~2 years into the test. At the three-year point of the test, the temperature at the canister mid-height started to decrease due to failure of some heater elements.

Table 2-2. Composition of groundwater used in the experiment.

Date	Na mg/L	K mg/L	Ca mg/L	Mg mg/L	HCO_3 mg/L	Cl mg/L	SO_4 mg/L	SO_4-S mg/L	Br mg/L	F mg/L	Si mg/L
1999-04-12	1,830.0	16.8	1,284.0	96.8	114.0	5,530.0	363.0	112.0	36.1	1.56	4.70
1999-10-04	1,730.0	20.7	987.0	123.1	147.0	4,590.0	382.0	115.0	25.3	1.31	5.50
2001-09-26	1,390.0	30.7	286.0	125.0	195.0	2,540.0	261.0	98.9	12.1	1.20	5.51
2002-09-24	1,590.0	27.8	629.0	120.0	164.0	3,841.3	316.2	99.6	21.9	1.64	5.40
2004-09-21	1,480.0	29.3	611.0	106.0	170.0	3,360.0	325.0	105.0	29.8	1.45	5.63
Mean	1,604.0	25.1	759.4	114.2	158.0	3,972.3	329.5	106.1	25.0	1.43	5.35
Std	179.11	6.01	384.10	12.24	30.02	1,145.81	46.8	7.23	8.98	0.18	0.37

Date	Fe_{TOT} mg/L	Fe(II) mg/L	Mn mg/L	Li mg/L	Sr mg/L	pH mg/L	COND mg/L	DOC mg/L	NH_4-N mg/L
1999-04-12	0.703	0.707	0.580	0.7000	16.10	7.40	1,250.0	4.5	0.3978
1999-10-04	0.912	0.912	0.845	0.4975	14.00	7.40	1,310.0	5.4	0.6766
2001-09-26	0.937	0.941	0.683	0.1200	4.39	7.50	830.0	5.6	0.6900
2002-09-24	0.897	0.904	0.667	0.3780	9.95	7.45	1,178.0	5.1	0.8547
2004-09-21	0.843	0.841	0.590	0.4070	9.51	7.45	1,020.0	5.6	0.9430
Mean	0.858	0.861	0.674	0.421	10.79	7.4	1,117.6	5.2	0.712
Std	0.09	0.09	0.11	0.21	4.52	0.04	193.93	0.46	0.21

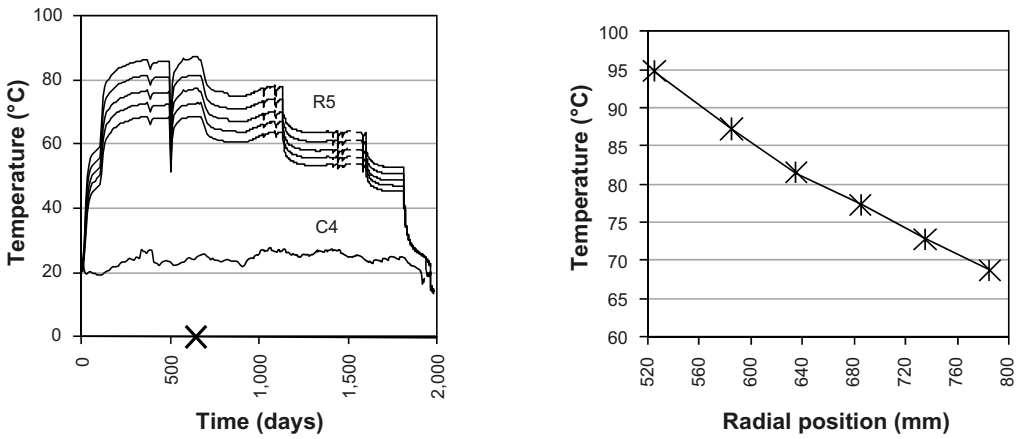

Figure 2-3. *Left: The measured temperature evolution in the buffer at different radii in R5 and in the center of C4. Right: The measured temperature profile in the buffer at canister mid-height (in Ring 5) at day 643 (indicated in the left figure). The temperature at 525 mm (the canister surface) has been calculated from assuming perfect radial heat flow.*

2.3 Excavation phase

The excavation phase started in October 2005 with the removal of the rock anchors, steel lid and concrete plug. The buffer was then sampled above canister mid-height (blocks C4 to R6). The retrieving technique was tested from canister mid-height and downwards (blocks R5 to C1). The canister was gripped by the canister lid and lifted up to the tunnel floor. The retrieval phase is described in Eng (2008).

The state of the bentonite buffer at the excavation (Figure 2-4) was determined by Johannesson (2007) in terms of water content, dry density and degree of water saturation, as described in Appendix 2. In block R7, about mid-height of the canister, the buffer was fully water saturated in its final state (the pellet slot is excluded in the description below) and had an approximately homogeneous dry density of 1,600 kg/m^3. In block C4, above the canister, the buffer had a degree of water saturation of 80% and a dry density of 1,650 kg/m^3 in the central parts, and was fully water saturated and had a dry density of 1,500 kg/m^3 at the parts close to the slot with pellets. The original densities at these locations are provided in Table 2-1.

2.4 Sampling

Bentonite from the CRT buffer had been stored as cores or as large block pieces in evacuated plastic bags since the retrieval in 2006. In 2007, block R7 from the heated section (T_{max} ~95°C) and block C4 from the cool section (T_{max} ~30°C) of the buffer were sampled.

Block C4 from the top of the buffer (cf. Figure 2-1) had a diameter of 1.65 m. Cores (length 50 cm, Ø 50 mm) from approximately equally spaced positions along the block radius were sampled. Each sample represented 2–5 cm of the radius.

Block R7 had an inner diameter of ~1.10 m and an outer diameter of ~1.65 m. Test samples were taken from cores (length 50 cm, Ø 50 mm) from the outer part of the block, whereas test samples of the innermost decimeters of the block were sampled radially along a section of the block, each sample representing 2–5 cm of the block radius. The bentonite pellets added at the installation to seal between the blocks and the borehole wall were excluded in the sampling.

Individual samples were labeled according to the general nomenclature ***block id : angle : radial distance (mm)***, e.g. R7 : 230 : 580. The corresponding reference sample was labeled e.g. R7R.

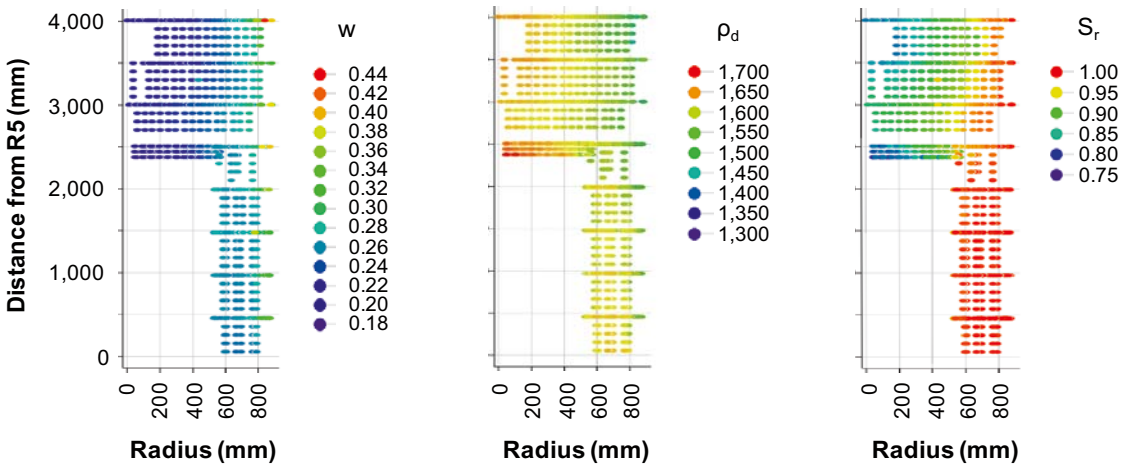

Figure 2-4. *Buffer state at excavation: water content w (-), dry density ρ_d (kg/m^3), and degree of saturation S_r (-).*

3 Chemical-mineralogical analyses

3.1 Material and methods

3.1.1 Sampling and sample labeling

The chemical and mineralogical composition was determined using the analytical methods listed in Table 3-1. A total of nine cores (length 50 cm, Ø 50 mm) from approximately equally spaced positions along the block radius were sampled from block C4. Each sample represented ~ 3 cm of the radius.

Table 3-1. Analytical methods and labeling of the bentonite samples of the CRT buffer. EA = element analysis, CEC = cation exchange capacity, XRD = X-ray diffraction analysis, EC = exchangeable cations, WS = water-soluble salts. b = bulk sample, c = fine clay fraction < 1 µm.

Analysis	Block	Angle°	Radial distance from centre, mm	Material
EA, CEC	C4	225	35	b and c
EA, CEC	C4	225	180	b and c
EA, CEC	C4	225	285	b and c
EA, CEC	C4	225	382	b and c
EA, CEC	C4	225	478	b and c
EA, CEC	C4	225	571	b and c
EA, CEC	C4	225	666	b and c
EA, CEC	C4	225	752	b and c
EA, CEC	C4	315	795	b and c
EC, WS and XRD	C4	225	35	b
EC, WS and XRD	C4	225	180	b
EC, WS and XRD	C4	225	285	b
EC, WS and XRD	C4	225	382	b
EC, WS and XRD	C4	225	478	b
EC, WS and XRD	C4	225	571	b
EC, WS and XRD	C4	225	666	b
EC, WS and XRD	C4	225	752	b
EC, WS and XRD	C4	315	795	b
EA, CEC and XRD	R7	300	525	b and c
EA, CEC and XRD	R7	300	545	b and c
EA and CEC	R7	300	580	b and c
EA, CEC and XRD	R7	300	615	b and c
EA, CEC and XRD	R7	300	650	b and c
EA and CEC	R7	315	695	b and c
EA, CEC and XRD	R7	315	765	b and c
EA, CEC and XRD	R7	315	790	b and c
EC and WS	R7	300	525	b
EC and WS	R7	300	545	b
EC, WS and XRD	R7	300	580	b
EC and WS	R7	300	615	b
EC and WS	R7	300	650	b
EC, WS and XRD	R7	315	695	b
EC and WS	R7	315	765	b
EC and WS	R7	315	790	b
EA, CEC	C4R			b and c
EC, WS and XRD	C4R			b
EA, CEC and XRD	R7R			b and c
EC and WS	R7R			b

A total of eight samples were taken from block R7. Three samples were taken from cores from the outer part of the block, whereas the innermost 14 cm of the block was sampled contiguously at four positions in a section of the block, each sample representing approximately 3 cm of the block radius. To increase the spatial resolution at the canister, a 1–2 mm thick layer of the inner surface of block R7 (sample R7 525) was scraped off and treated as a separate sample. The bentonite pellets added at the installation to seal between the blocks and the borehole wall were excluded in the sampling.

Individual samples were labeled according to the general nomenclature (see 2.4) with addition of a suffix b (for bulk) or c (for clay), because both the bulk material and the fraction < 1μm were analyzed. The corresponding reference sample was labeled e.g. R7Rb (or c).

3.1.2 Sample preparation

Both the bulk material and the fine clay fraction (equivalent diameter < 1 μm) were analyzed for mineralogy, cation exchange capacity, and chemical composition (cf. Table 3-1). The bulk sample was not subject to any pre-treatments prior to analysis, apart from drying at 60°C and grinding.

In order to facilitate separation of the fine clay fraction, the bentonite was first suspended in deionized water and the suspension was left long enough to allow sedimentation of coarse particles and dissolution of soluble salts. The suspension was thereafter collected and the clay was converted to homo-ionic Na-clay by two additions of 1 M NaCl solution followed by centrifugation and decantation of the clear supernatant. Excess salt was removed by centrifuge-washings followed by dialysis (Spectrapore 3, 3500 MWCO dialysis membrane) against deionized water until the electrical conductivity of the external water remained < 10 μS/cm for five days. After completing dialysis the slurry was dispersed in deionized water and centrifuged with a centrifugation time/speed calculated by use of Stokes' Law to correspond to a particle separation at an equivalent diameter of 1 μm. The supernatants were concentrated by evaporation at 60°C. The technique applied has been proven to produce homoionic smectite from a number of different bentonites with low contents of soluble calcium/magnesium minerals, such as MX-80 (Karnland et al. 2006).

3.1.3 Bentonite composition

The chemical composition of the bulk bentonite and of the Na-saturated < 1μm fraction was determined at an ISO 9001:2000 accredited laboratory (ACME Analytical Laboratories, Vancouver, Canada). The < 1μm fraction, instead of the conventional < 2μm fraction, was chosen for these analyses to get as pure a smectite fraction as possible, thereby making the element allocation in formula calculations less ambiguous. Similarly, the clay was saturated with one single, non-structural cation – in this case sodium – to make the allocation of cations to exchange and structural sites, respectively, less ambiguous.

After digestion of the samples using standard techniques for silicate analysis ($LiBO_2/Li_2B_4O_7$ fusion/ dilute nitric acid digestion) major and some minor and trace elements were determined using ICP-AES. A separate analysis of Mo was made by the use of ICP-MS.

Loss on ignition (LOI) was determined as the difference in weight of the samples dried at 105°C and after ignition at 1,000°C.

Total carbon and total sulphur were determined at the same laboratory by evolved gas analysis. The sample was combusted in a Leco furnace, equipped with IR-detectors for CO_2 and SO_2. Acid-soluble carbon was determined as CO_2 evolved on direct treatment with hot 15% HCl. Sulfate was determined after ignition of a sub-sample at 800°C.

3.1.4 Aqueous leachates

The distribution of soluble chlorides and sulfates was determined in water extracts of the bulk bentonite. The dried and ground bentonite was dispersed in deionised water (solid:solution ratio 1:100) by ultrasonic treatment for 30 minutes and stirring overnight. The suspension was left for 5 days at room temperature to allow equilibration and sedimentation of the coarse matter. After phase separation by centrifugation and filtration (0.8 and 0.2 μm syringe filters Acrodisc PF), major anions (Cl^-, SO_4^{2-}, NO_3^- PO_4) were determined by use of ion chromatography (IC) at the Department of Ecology, Lund University.

3.1.5 Exchangeable cations and cation exchange capacity (CEC)

The exchangeable cations of the bulk bentonite were extracted into alcoholic ammonium chloride solution (~0.15M NH_4Cl in 80% ethanol) according to a procedure originally recommended for CEC determinations of gypsiferous/calcareous soils (e.g. Belyayeva 1967, Jackson 1975). An alcoholic solution was used to minimize dissolution of gypsum and calcite, which are soluble in aqueous solutions. Ideally, i.e. when there is a minimum of easily soluble salts, such as chlorides and sulfates/carbonates of alkali metals, the sum of extracted cations should be equivalent to the CEC of the sample.

0.8 g of the ground sample was shaken for 30 minutes in approximately one third of a total volume of 50 ml of the extractant. After centrifugation the supernatant was collected. This treatment was repeated twice. After evaporation of the alcohol and adjustment of the volume with deionized water, the concentration of Ca, Mg, Cu, Na and K was determined by use of an ICP-AES equipment at the Department of Ecology, Lund University. The water content of the bentonite was determined for a separate sample.

The cation exchange capacity (CEC) of bulk materials and of fine clay fractions (< 1 μm) was determined by exchange with copper(II)triethylenetetramine following the procedure of Meier and Kahr (1999) modified according to Ammann et al. (2005) to ensure complete exchange. The ground sample (400 mg) was dispersed in 50 ml deionized water by ultrasonic treatment and shaking overnight. 20 ml of 15 mM Cu(II)-triethylenetetramine solution was added to the suspension, which was left to react for 30 minutes on a vibrating table. After centrifugation the absorbance at 620 nm of the supernatant was measured using a spectrophotometer (Shimadzu) and CEC calculated on the basis of the uptake of Cu by the clay. The water content of the clay was determined for a separate sample dried at 105°C for 24 hours. All CEC determinations were duplicated.

3.1.6 X-ray diffraction analysis

The mineralogical composition was determined by X-ray diffraction analysis of randomly oriented powders of the bulk samples. The specimens were prepared of the bulk material ground to a grain-size < 10 μm and scanned in the 2θ interval 2–66° with a step-size of 0.02° 2θ and a scanning speed of 1° 2θ/min.

The fine clay fraction (< 1 μm) of six of the samples from block R7 was also X-ray scanned as aggregates with maximised preferred orientation of the clay minerals. Since the diffraction characteristics of smectites depend on the type of interlayer cations among other factors, the fine clay fractions were saturated with Mg (0.5M $MgCl_2$) in order to give unambiguous diffraction characteristics. After removal of excess salt by centrifuge-washings, oriented aggregates were prepared of the clay slurry according to the "smear-on-glass" method and dried at room temperature. The mounts were X-ray scanned in the 2θ interval 2–36° with a step-size of 0.02° 2θ and a scanning speed of 1° 2θ/min. The block samples from the central, mid- and peripheral positions were re-scanned after solvation with ethylene glycol at 60°C for 48 hours to test the swelling properties. A Seifert 3000 TT X-ray diffractometer with CuKα radiation and automatic slits was used for the X-ray diffraction analyses.

3.2 Results

3.2.1 Yields of fine clay

The size separation yielded between 74 and 83% of fine clay (< 1μm) for all samples but one (yield = 100·mass of < 1μm fraction/mass of bulk sample). The exception was the sample of the inner surface of block R7, for which the yield of fine clay was 56% (Figure 3-1). Neither the CEC data (Table 3-4) nor the crystal chemistry (Table 3-7) gave any obvious indication that the proportion or the composition of the clay minerals was drastically changed in this sample. It is therefore believed that the low yield of fine clay was an effect of contamination of the sample by an oil-based lubricant that had been applied to the walls of the mould used in the manufacturing of the blocks.

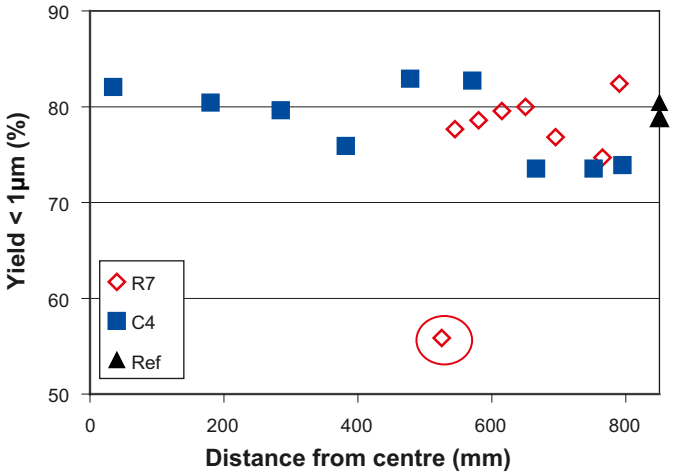

Figure 3-1. *Yield of the fraction < 1 µm from the samples of block C4 and R7. The results for two reference samples are shown at position 850 mm. Encircled sample is from the contact surface bentonite/Cu-canister in block R7.*

3.2.2 Aqueous leachates

The content of the major soluble anions determined by leaching the bentonite in water are given in Table 3-2 as mg/g dry clay. The concentrations of chloride and sulfate have been recalculated as molar concentrations (mM) in Figure 3-2, in order to facilitate comparison with the mean concentrations in the groundwater at Äspö (cf. Table 2-2), which are included in the figure. The molar concentrations were calculated using the water content of the samples listed in Table 3-2.

The inner 40 cm of block C4 was not fully water saturated at the time of retrieval (degree of saturation < 85%), which is reflected by a steep gradient in the chloride concentration towards the centre of the block, where the concentration remained almost the same as that of the reference bentonite. In the fully saturated block R7, the hydration by groundwater resulted in an increased but constant concentration of chloride, which suggests that the chloride concentration was apparently unaffected by the evaporation and condensation cycling that is expected to occur during the saturation of the heated part of a bentonite buffer (Arcos et al. 2010). The chloride concentration is, however, still only half of that of the Äspö groundwater (cf. Table 2-2) after the test period, which may simply be a dilution effect but is qualitatively also predicted by ion equilibrium theory (Birgersson and Karnland 2009).

The sulphate concentration in the water extracts of the MX-80 references (Figure 3-2) is much higher than that of the Äspö groundwater, demonstrating that the inventory of gypsum in the MX-80 bentonite is the primary sulphate source. The sulphate concentration in block C4 is more or less constant and the same as that of the reference bentonite. In contrast, the heated block R7 displays a sulphate maximum at the canister, and XRD analysis confirms that anhydrite ($CaSO_4$) has formed here. The calcium

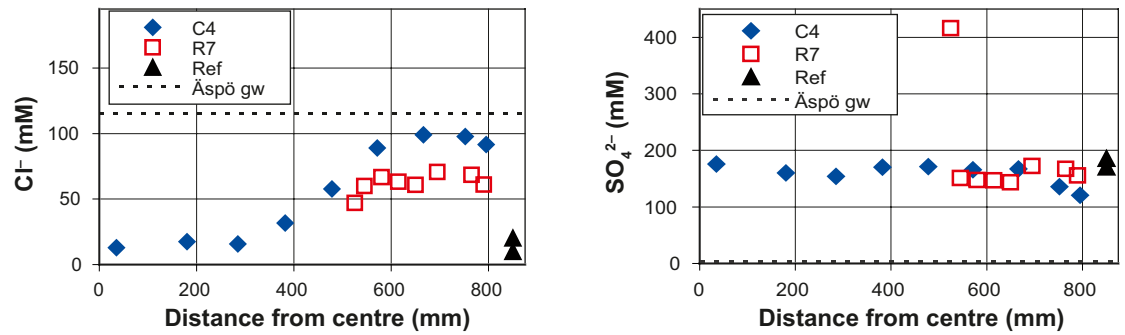

Figure 3-2. *The radial distribution of Cl^- and SO_4^{2-} (mM) in water extracts of bulk samples from block C4 and R7 of the CRT buffer. Hatched line shows the mean concentration in the groundwater at Äspö during the period 1999–2004. The concentration of the reference samples is plotted at position 850 mm.*

Table 3-2 Major anions (mg/g dry clay) extracted by dispersion of bentonite in deionized water in a solid:liquid ratio of 1:100. Data for block C4 and R7 from the CRT buffer and reference samples. The water-content (w) listed in the right column were used in calculations of molar concentrations.

Sample id	Cl	NO_3-N mg/g dry clay	SO_4-S	w
C4 225 035b	0.09	0.06	1.16	0.206
C4 225 180b	0.13	0.06	1.08	0.210
C4 225 285b	0.12	0.07	1.06	0.215
C4 225 382b	0.25	0.07	1.21	0.222
C4 225 478b	0.48	0.07	1.28	0.233
C4 225 571b	0.78	0.06	1.32	0.248
C4 225 666b	0.94	0.04	1.44	0.269
C4 225 752b	1.05	0.03	1.32	0.303
C4 315 795b	1.15	0.03	1.37	0.354
C4 Rb	0.06	0.06	1.10	0.185
R7 300 525b	0.44	0.04	3.49	0.262
R7 300 545b	0.55	0.04	1.25	0.259
R7 300 580b	0.61	0.05	1.21	0.256
R7 300 615b	0.57	0.04	1.20	0.255
R7 300 650b	0.55	0.04	1.17	0.254
R7 315 695b	0.64	0.04	1.42	0.256
R7 315 765b	0.62	0.04	1.38	0.257
R7 315 790b	0.58	0.04	1.35	0.270
R7 Rb	0.17	0.05	1.01	0.171

sulfates, which have temperature dependent solubility, have clearly been influenced by the gradients in temperature and hydration that prevailed during the test period. Despite differences in the experimental conditions, the results conform with those reported for a medium-scale field test with MX-80 bentonite heated at 130°C (Karnland et al. 2009), and also with laboratory experiments with FEBEX bentonite heated at 100°C (Fernández and Villar 2010). Both studies demonstrated that calcium sulfate was leached from the bentonite in the proximity of the hydration source and accumulated in the heated part of the bentonite

3.2.3 Exchangeable cations and cation exchange capacity

The data on the cations extracted by exchange with ammonium in alcoholic solution are summarized in Table 3-3 and plotted in Figure 3-3. In general, there is a fairly good match between the sum of cations and the CEC of the sample (Table 3-4), which indicates that soluble salts contribute little to the extracted cation population. The proportions between the major exchangeable cations, K, Na, Mg and Ca, in the block samples are essentially the same as in the reference samples, i.e. around two thirds of the exchange sites are occupied by sodium and calcium is second most abundant. A small decrease in the proportion of Mg in the peripheral parts of both blocks suggests replacement of some exchangeable Mg, mainly by Ca, which would be an expected effect of the equilibration of the cation pool against a Na-Ca-dominated groundwater.

Cu concentrations in clear excess of the analytical detection limit were found only in the extract of the sample of the bentonite/Cu-tube interface in the heated block. The extractable amount of Cu is << 1% of the total exchangeable cation pool and makes up less than 8% of the maximum available amount of Cu (cf. Table 3-5).

The cation exchange capacity of bulk samples and of fractions < 1 μm are compiled in Table 3-4 and the mean values are plotted against the radial distance in Figure 3-4. The CEC value of the reference bentonites, 81 meq/100 g, matches the Cu-CEC value previously reported for the bentonite MX-80 (Karnland et al. 2006, 2009). No significant difference can be seen among the block samples and those variations that exist appear to be random and independent of the position of the sample in the buffer. The same is true for the CEC of the < 1 μm fractions.

Table 3-3. Exchangeable cations of the samples from block C4 and R7 of the CRT buffer, together with the reference samples for the blocks. Cations extracted by exchange with $NH4^+$ in alcoholic solution.

Sample id	Ca		Cu	K		Mg		Na		Σ cations
	meq/100 g	%	meq/100 g	meq/100 g	%	meq/100 g	%	meq/100 g	%	meq/100 g
C4 225 035b	16	21	0.00	1.3	1.7	4.4	6	56	72	78
C4 225 180b	16	21	0.00	1.4	1.8	4.4	6	55	71	77
C4 225 285b	17	22	0.01	1.4	1.8	4.8	6	54	70	77
C4 225 382b	17	22	0.00	1.4	1.8	5.1	6	54	70	78
C4 225 478b	18	22	0.00	1.4	1.8	5.3	7	55	70	79
C4 225 571b	18	22	0.00	1.4	1.8	5.2	6	55	69	80
C4 225 666b	17	22	0.00	1.5	1.9	5.2	6	55	70	79
C4 225 752b	19	24	0.01	1.7	2.1	4.6	6	56	69	81
C4 315 795b	18	23	0.01	1.5	2.0	2.9	4	55	71	77
C4 Rb	18	22	0.00	1.6	1.9	7.2	9	54	67	81
R7 300 525b	17	22	0.09	1.2	1.6	6.8	9	53	68	78
R7 300 525b-2	19	23	0.11	1.5	1.8	7.5	9	53	66	81
R7 300 545b	18	22	0.00	1.6	1.9	6.0	7	56	69	81
R7 300 580b	18	23	0.00	1.6	1.9	5.8	7	56	68	81
R7 300 615b	18	23	0.01	1.4	1.8	5.3	7	53	68	77
R7 300 615b-2	18	23	0.00	1.6	1.9	5.6	7	54	68	80
R7 300 650b	18	23	0.00	1.6	2.0	5.7	7	55	68	81
R7 315 695b	18	23	0.01	1.4	1.8	5.5	7	55	69	79
R7 315 765b	18	23	0.01	1.4	1.8	4.8	6	53	69	77
R7 315 765b-2	19	23	0.00	1.6	2.0	5.2	6	56	68	82
R7 315 790b	18	24	0.01	1.4	1.8	4.2	5	54	69	78
R7 Rb	18	22	0.02	1.5	1.8	7.0	9	55	68	81
R7 Rb-2	17	21	0.00	1.5	1.9	6.9	9	54	68	80

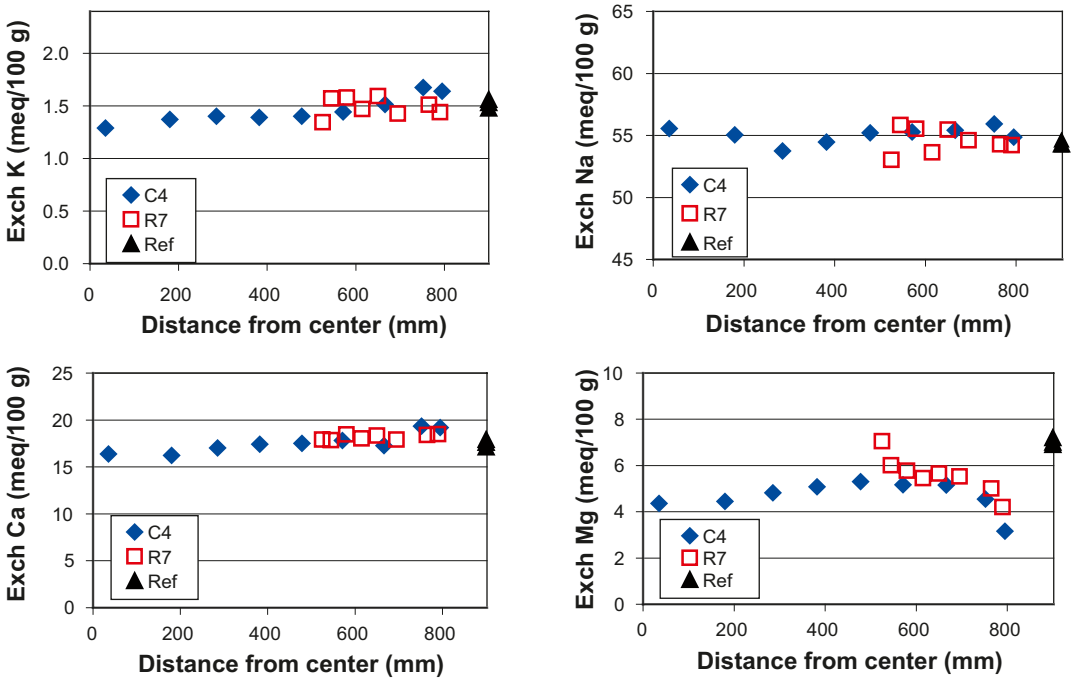

Figure 3-3. *Exchangeable K, Na, Ca and Mg of the bentonite from block C4 and R7 of the CRT buffer. Reference samples are plotted at the position 900 mm.*

Table 3-4. Cation exchange capacity (meq/100 g) of the bulk samples and of the fraction < 1µm from block C4 and R7 of the CRT buffer, together with the reference samples for the blocks. Values within parantheses are discussed in the text.

Sample id	CEC bulk sample meq/100 g dry matter		Mean	Sample id	CEC < 1µm fraction meq/100 g dry matter		Mean
C4 225 035b	80	78	79	C4 225 035c	92	93	93
C4 225 180b	82	81	82	C4 225 180c	93	92	92
C4 225 285b	81	81	81	C4 225 285c	93	93	93
C4 225 382b	82	81	82	C4 225 382c	93	92	93
C4 225 478b	80	81	81	C4 225 478c	91	93	92
C4 225 571b	81	79	80	C4 225 571c	92	90	91
C4 225 666b	81	81	81	C4 225 666c	93	91	92
C4 225 752b	81	82	82	C4 225 752c	93	94	93
C4 225 795b	80	80	80	C4 225 795c	93	90	92
C4 Rb	82	81	82	C4 Rc	90	93	92
R7 300 525b	(79	79	79)	R7 300 525c	(90	91	91)
R7 300 545b	80	81	81	R7 300 545c	93	95	94
R7 300 580b	81	80	80	R7 300 580c	95	94	95
R7 300 615b	81	81	81	R7 300 615c	94	94	94
R7 300 650b	81	81	81	R7 300 650c	93	91	92
R7 315 695b	80	80	80	R7 315 695c	94	94	94
R7 315 765b	80	80	80	R7 315 765c	92	93	93
R7 315 790b	81	81	81	R7 315 790c	92	92	92
R7 Rb	81	81	81	R7 Rc	92	93	92

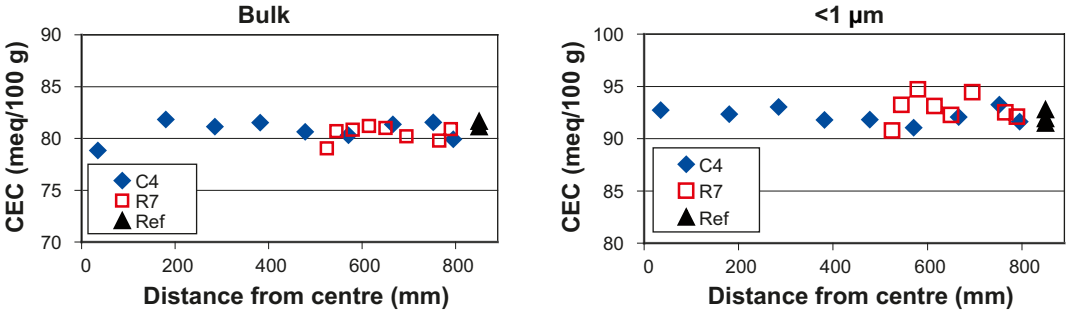

Figure 3-4. CEC of the bulk bentonite and of the < 1µm fraction of block C4 and R7 of the CRT buffer. Reference samples are plotted at the position 850 mm.

CEC values within parentheses in Table 3-4 are for the sample of the inner surface of block R7, which contains ~2.5% "organic" carbon believed to be derived from the oil-based lubricant used in block manufacturing. Therefore, these CEC values must be considered uncertain, both because of the dilution effect, but also because the contaminant itself may produce artifacts in the CEC determination.

3.2.4 Bentonite composition

The chemical composition of the samples is given in Table 3-5 (bulk samples) and Table 3-6 (Na-saturated < 1 µm fractions).

Calcite and gypsum are trace constituents (1–2%) in the bentonite MX-80 but attention is paid to these minerals because of their temperature-dependent solubility, which will influence their behavior under the non-isothermal conditions and the hydration gradients that prevail during the water saturation of the buffer.

The total carbon content of the reference bentonite is 0.29% (DL = 0.02%) and the content of acid-soluble carbon, which is derived mainly from carbonate phases, is 0.13% C. The remaining, acid-insoluble fraction normally emanates from mature organic matter.

The concentration of total sulphur in the reference bentonite is 0.28% (DL = 0.02%). According to the data on water-soluble salts, 40–50% of the total sulphur content originates from water-soluble minerals, the most abundant being gypsum ($CaSO_4 \cdot 2H_2O$). The source of the remaining fraction, 0.10–0.15% S, is sulphide and possibly low solubility sulphates (e.g. $BaSO_4$).

After the hydrothermal exposure, the distribution of the acid-soluble carbon fraction (Figure 3-5 left) varies between 0.10 and 0.14% C in both blocks. A tendency of decreasing values may be present in the inner part of block R7 but the range of variation is close to the analytical resolution.

Also the acid-insoluble fraction of carbon (Figure 3-5 middle) is more or less constant in both blocks, the only exception being the sample from the bentonite/Cu-tube interface in block R7, which has a conspicuously high content of "organic carbon". However, in this case, the acid-insoluble carbon fraction most likely originates from the lubricant Molykote® BR2+, which was applied to the walls of the moulds used in the manufacturing of the blocks. According to the specification from the producer (Dow Coring), the lubricant is based on distillates of mineral oil with a thickener of lithium soap and also contains MoS_2 and Zn-dialkyldithiophosphate. As shown in the chemical data (Table 3-5 and Table 3-6), both the bulk bentonite and the fine clay fraction of sample 525 from the bentonite/Cu-tube interface have elevated concentrations of C, Mo, P and Zn (evaluated on an ignited basis), i.e. a combination of elements that clearly suggests adsorption of the lubricant on the bentonite (Li is not included in the analysis because Li-borate is used for the sample digestion). The lubricant is a candidate source also of some sulfur, but the amount is most likely insufficient to explain the twofold increase in total sulfur near the canister (Figure 3-5 right), where anhydrite formed.

A supplementary analysis of total carbon made on 2.5-mm thick, contiguous samples from the innermost 25 millimetres of block R7 (Figure 3-6) suggests that the bentonite is contaminated to a depth of approximately 0.5 cm. The chemical composition of the < 1 µm fraction shows that the fractionation of the bentonite by size does not reduce the "organic" carbon content, suggesting that the lubricant adheres preferentially to surfaces of clay particles.

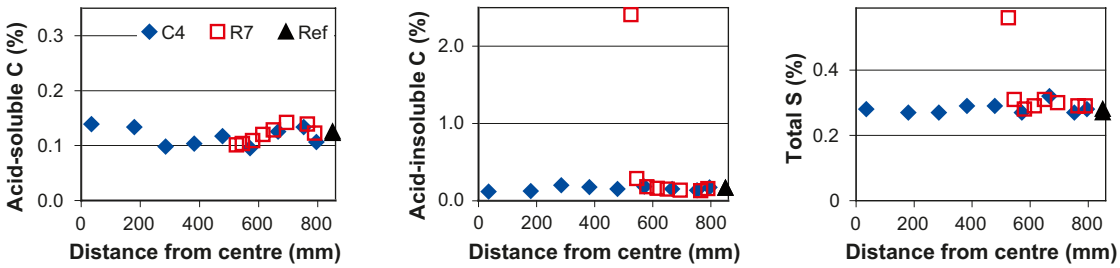

Figure 3-5. *Acid-soluble (left), acid-insoluble carbon (middle) and total sulfur (right) in bulk samples of block C4 and R7 of the CRT buffer. Values for the references are shown at the distance 850 cm.*

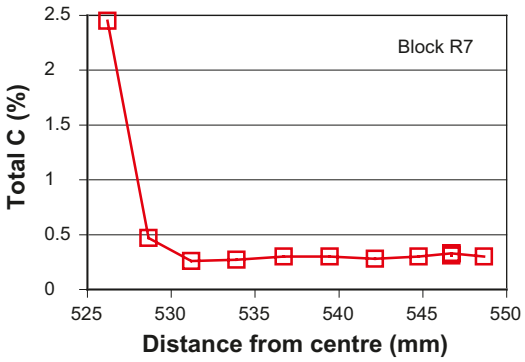

Figure 3-6. *The distribution of total carbon in the interval 0–25 mm at the canister in block R7.*

Table 3-5. Chemical composition of the bulk bentonite samples from blocks C4 and R7 of the CRT buffer together with the reference samples for the blocks. Major and minor/trace elements by ICP-AES, Mo by ICP-MS, C and S by evolved gas analysis.

Sample id	SiO_2 %	Al_2O_3 %	Fe_2O_3 %	MgO %	CaO %	Na_2O %	K_2O %	TiO_2 %	P_2O_5 %	MnO %	Cr_2O_3 %	Mo %	Ba ppm	Cu ppm	Zn ppm	Ni ppm	Co ppm	Sr ppm	Zr ppm	Ce ppm	Y ppm	Nb ppm	Sc ppm	Ta ppm	LOI %	Sum %	Ctot %	Stot %	$C\text{-}CO_2$ %	$S\text{-}SO_4$ %
C4 225 035b	62.8	19.96	3.55	2.49	1.18	2.17	0.54	0.14	0.04	0.01	0.002	<.001	425	5	69	11	5	292	201	91	46	28	6	5	7.0	100.1	0.26	0.28	0.14	0.13
C4 225 180b	62.5	19.83	3.54	2.49	1.12	2.08	0.49	0.14	0.03	0.01	0.001	<.001	262	10	51	5	5	261	197	94	45	28	6	6	7.6	99.9	0.26	0.27	0.13	0.13
C4 225 285b	62.7	19.87	3.54	2.53	1.17	2.07	0.50	0.14	0.06	0.01	0.006	<.001	289	5	93	5	8	286	192	91	46	25	6	5	7.2	99.9	0.3	0.27	0.10	0.16
C4 225 382b	61.9	19.69	3.44	2.44	1.19	2.11	0.52	0.14	0.05	0.01	0.004	<.001	547	5	88	5	5	289	200	91	45	24	6	5	8.4	100.1	0.28	0.29	0.10	0.15
C4 225 478b	62.9	19.90	3.63	2.47	1.22	2.12	0.52	0.14	0.05	0.01	0.017	<.001	306	5	125	5	5	271	195	83	46	31	6	5	7.0	100.1	0.27	0.29	0.12	0.14
C4 225 571b	63.2	19.80	3.54	2.49	1.2	2.14	0.53	0.14	0.03	0.01	0.002	<.001	321	5	95	5	5	273	192	92	47	26	5	5	6.9	100.1	0.28	0.27	0.10	0.16
C4 225 666b	63.0	19.98	3.57	2.49	1.15	2.15	0.51	0.14	0.04	0.01	0.001	<.001	292	5	59	5	5	277	188	89	46	28	6	5	6.9	100.1	0.28	0.32	0.13	0.17
C4 225 752b	62.8	20.01	3.64	2.45	1.25	2.17	0.54	0.14	0.05	0.01	0.001	<.001	299	5	59	6	5	293	194	98	47	26	6	7	6.9	100.1	0.27	0.27	0.13	0.16
C4 225 795b	62.4	20.23	3.52	2.47	1.31	2.24	0.54	0.14	0.05	0.01	0.001	<.001	262	5	91	5	5	301	194	98	47	33	6	8	7.0	100.1	0.28	0.28	0.11	0.17
R7 300 525b	60.8	19.09	3.43	2.47	1.74	2.07	0.49	0.14	0.07	0.01	0.001	0.02	258	414	374	5	5	254	185	89	44	30	6	5	9.4	99.9	2.51	0.56	0.10	0.45
R7 300 545b	62.8	20.13	3.55	2.51	1.19	2.2	0.55	0.15	0.06	0.01	0.003	<.001	344	5	85	5	5	300	196	95	48	33	6	5	6.8	100.1	0.39	0.31	0.10	0.19
R7 300 580b	62.7	20.14	3.58	2.48	1.21	2.23	0.59	0.14	0.05	0.01	0.006	<.001	360	9	71	10	5	293	199	93	47	24	6	5	6.8	100.1	0.29	0.28	0.11	0.17
R7 300 615b	62.6	20.10	3.58	2.45	1.22	2.22	0.56	0.15	0.06	0.01	0.001	<.001	321	5	151	5	5	295	197	95	47	32	6	5	7.0	100.1	0.28	0.29	0.12	0.17
R7 300 650b	62.7	20.03	3.65	2.46	1.18	2.21	0.55	0.14	0.05	0.01	0.006	<.001	465	5	75	5	5	299	200	83	46	32	6	5	6.9	100.1	0.28	0.31	0.13	0.16
R7 315 695b	62.6	19.87	3.60	2.46	1.31	2.14	0.53	0.14	0.04	0.01	0.005	<.001	300	5	73	12	5	296	198	77	47	22	6	10	7.1	99.9	0.28	0.30	0.14	0.17
R7 315 765b	62.2	20.14	3.53	2.48	1.25	2.21	0.55	0.14	0.06	0.01	0.005	<.001	365	5	87	5	5	304	202	95	48	30	6	8	7.4	100.1	0.27	0.29	0.14	0.16
R7 315 790b	62.6	20.29	3.57	2.47	1.25	2.25	0.56	0.15	0.04	0.01	0.004	<.001	287	5	86	5	5	298	199	98	48	28	6	5	6.8	100.1	0.28	0.29	0.12	0.17
R7 Rb	62.3	20.44	3.53	2.52	1.24	2.17	0.56	0.14	0.05	0.01	0.001	<.001	294	5	102	5	5	292	195	94	47	31	6	5	7.0	100.1	0.29	0.28	0.12	0.13
C4 Rb	62.8	20.29	3.64	2.53	1.20	2.20	0.53	0.14	0.04	0.01	0.001	<.001	282	5	71	5	7	284	197	86	47	32	6	5	6.6	100.1	0.29	0.27	0.13	0.14

Table 3-6. Chemical composition of the Na-saturated fine clay fraction (< 1 µm) of bentonite samples from blocks C4 and R7 of the CRT buffer together with the reference samples for the blocks. Major and minor/trace elements by ICP-AES, Mo by ICP-MS, C and S by evolved gas analysis.

Sample id	SiO_2 %	Al_2O_3 %	Fe_2O_3 %	MgO %	CaO %	Na_2O %	K_2O %	TiO_2 %	P_2O_5 %	MnO %	Cr_2O_3 %	Mo %	Ba ppm	Cu ppm	Zn ppm	Ni ppm	Co ppm	Sr ppm	Zr ppm	Ce ppm	Y ppm	Nb ppm	Sc ppm	Ta ppm	LOI %	Sum %	Ctot %	Stot %
C4 225 035c	63.7	20.55	3.75	2.54	0.11	2.39	0.08	0.1	0.03	0.01	< .001	< 0.001	29	< 5	34	< 5	< 5	33	145	86	38	22	6	7	6.5	99.84	0.15	0.02
C4 225 180c	63.6	20.77	3.79	2.63	0.11	2.46	0.07	0.1	0.02	< .01	< .001	< 0.001	24	< 5	41	< 5	< 5	33	149	88	37	27	6	< 5	6.4	99.99	0.13	0.02
C4 225 285c	63.5	21.09	3.74	2.62	0.10	2.48	0.07	0.1	0.03	< .01	< .001	< 0.001	23	5	33	8	< 5	32	145	87	35	21	6	< 5	6.1	99.85	0.14	0.01
C4 225 382c	63.2	21.26	3.77	2.63	0.1	2.46	0.07	0.1	0.03	0.01	< .001	< 0.001	22	< 5	33	< 5	< 5	31	147	86	37	24	6	< 5	6.3	99.99	0.13	0.02
C4 225 478c	63.4	21.15	3.69	2.65	0.11	2.51	0.07	0.1	0.02	0.01	< .001	< 0.001	23	< 5	31	< 5	< 5	34	148	90	38	23	6	8	6.2	99.98	0.15	0.02
C4 225 571c	63.8	20.95	3.81	2.65	0.12	2.44	0.07	0.1	0.03	0.01	< .001	< 0.001	25	< 5	32	< 5	6	34	147	93	38	22	6	< 5	6	99.98	0.14	0.02
C4 225 666c	63.0	21.29	3.77	2.64	0.10	2.48	0.07	0.1	0.02	0.01	< .001	< 0.001	22	< 5	32	5	< 5	32	146	87	34	23	6	< 5	6.5	99.98	0.13	0.01
C4 225 752c	63.4	20.93	3.75	2.59	0.11	2.4	0.06	0.09	0.02	0.01	< .001	< 0.001	21	< 5	30	< 5	< 5	34	144	84	33	26	6	< 5	6.6	99.99	0.14	0.02
C4 315 795c	63.8	20.82	3.8	2.62	0.10	2.5	0.06	0.1	0.02	0.01	< .001	< 0.001	19	< 5	24	< 5	< 5	31	145	89	33	25	6	< 5	6.1	99.99	0.12	0.01
R7 300 525c	61.5	20.47	3.75	2.52	0.07	2.41	0.07	0.09	0.02	0.01	< .001	0.004	14	497	352	< 5	< 5	15	145	83	36	26	6	< 5	8.8	99.85	2.60	0.03
R7 300 545c	63.4	20.76	3.88	2.62	0.11	2.46	0.08	0.1	0.02	0.01	< .001	< 0.001	27	12	85	< 5	< 5	36	148	88	38	22	6	5	6.5	99.99	0.27	0.01
R7 300 580c	63.3	20.93	3.86	2.62	0.10	2.52	0.07	0.1	0.02	0.01	< .001	< 0.001	24	< 5	38	< 5	6	32	148	88	38	25	6	< 5	6.4	99.98	0.13	0.01
R7 300 615c	63.3	20.97	3.82	2.61	0.13	2.47	0.08	0.1	0.03	0.01	< .001	< 0.001	28	< 5	31	< 5	< 5	42	148	89	39	26	6	7	6.4	99.98	0.15	0.02
R7 300 650c	63.8	20.68	3.84	2.61	0.11	2.49	0.08	0.1	0.02	0.01	< .001	< 0.001	28	< 5	29	7	6	32	150	94	39	25	6	< 5	6.2	100.0	0.14	0.02
R7 315 695c	63.3	21.02	3.91	2.61	0.12	2.53	0.07	0.1	0.02	0.01	< .001	< 0.001	32	< 5	32	< 5	7	35	149	86	34	24	6	7	6.2	99.98	0.16	0.02
R7 315 765c	63.1	20.89	3.83	2.6	0.1	2.57	0.06	0.1	0.04	0.01	< .001	< 0.001	21	< 5	30	< 5	< 5	32	147	84	35	19	6	7	6.6	99.98	0.15	0.02
R7 315 790c	63.5	20.94	3.79	2.52	0.12	2.49	0.09	0.1	0.02	0.01	< .001	< 0.001	31	< 5	30	< 5	< 5	36	149	91	40	21	6	8	6.4	99.99	0.17	0.02
R7 Rc	63.7	20.79	3.79	2.52	0.09	2.56	0.07	0.1	0.03	< .01	< .001	< 0.001	25	< 5	28	< 5	< 5	28	147	89	37	27	6	< 5	6.3	99.99	0.15	0.01
C4 Rc	63.8	21.01	3.74	2.58	0.10	2.6	0.06	0.1	0.03	< .01	< .001	< 0.001	23	8	27	< 5	7	30	146	88	37	24	6	< 5	5.9	99.99	0.19	0.02

The radial distribution of Cu within block R7 (Figure 3-7) shows that copper has been incorporated into the bentonite immediately adjacent to the canister. Despite prolonged washing/dialysis in the purification procedure, the < 1 µm fraction has a slightly higher Cu content (497 ppm) than the bulk bentonite (414 ppm), but treatment of a sub-sample of the clay with an acetic acid-sodium acetate buffer at pH 5 extracted much of the copper. The dissolution behavior indicates that copper is not a structural element in the smectite, but fixed in the clay in a water-insoluble form, possibly as adsorbed complexes or precipitates. The redox conditions in the buffer were not monitored during the field test, but corrosion of the copper canister may be explained by reactions during an early stage of the test when oxygen existed in the system, trapped in pores and dissolved in water.

3.2.5 Smectite composition

Based on the chemical composition of the < 1 µm fraction (Table 3-6), the molar proportions of the major structural elements in montmorillonite (Si, Fe, Al, Mg) have been calculated and plotted in the triangular diagram of Figure 3-8. Si in montmorillonite is uniquely located in the tetrahedral sheet. Fe and Mg are almost uniquely located in the octahedral sheet together with Al, but a fraction of the latter element is in general also tetrahedrally coordinated in montmorillonite. Fe has been assumed to be trivalent and has therefore been grouped with Al in the plot. As illustrated in the close-up of the plot (right) the geochemical variation among the samples is very small, suggesting that the montmorillonite composition has changed insignificantly in the 5-year test.

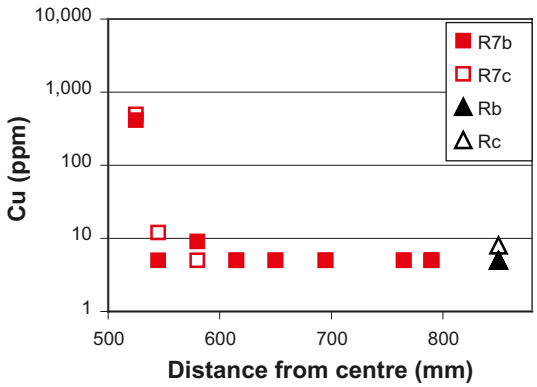

Figure 3-7. Plot of the Cu concentration in bulk samples and in fractions < 1 µm of block R7 versus the distance from the centre. Values for the reference samples are shown at position 850 mm.

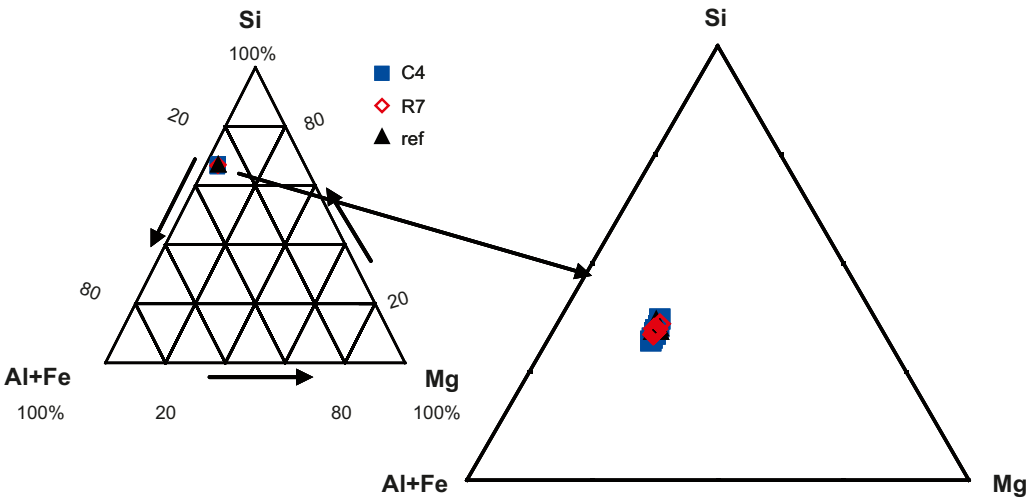

Figure 3-8. Triangular plot of the molar proportions (in percentages) of Si, Al+Fe and Mg in the Na-converted < 1 µm fractions.

Table 3-7. Calculated structural formula of the smectite in samples from block C4 and R7 of the CRT buffer. Calculations are based on the chemical data for the Na-saturated < 1µm fractions given in Table 3-6.

	C4 225 035	C4 225 180	C4 225 285	C4 225 382	C4 225 478	C4 225 666	C4 225 752	C4 315 795	C4 R
Si	8.00	8.00	7.98	7.95	7.97	7.94	7.99	8.00	7.99
Al	0.00	0.00	0.02	0.05	0.03	0.06	0.01	0.00	0.01
Σ tet	8.00	8.00	8.00	8.00	8.00	8.00	8.00	8.00	8.00
Al	3.10	3.08	3.10	3.11	3.11	3.11	3.11	3.08	3.10
Ti	0.01	0.01	0.01	0.01	0.01	0.01	0.01	0.01	0.01
Fe3+	0.36	0.36	0.35	0.36	0.35	0.36	0.35	0.36	0.35
Mg	0.48	0.49	0.49	0.49	0.49	0.49	0.48	0.49	0.48
Σ oct	3.95	3.94	3.95	3.97	3.96	3.97	3.95	3.94	3.94
Ca	0.02	0.01	0.01	0.01	0.01	0.01	0.01	0.01	0.01
Na	0.60	0.61	0.61	0.60	0.62	0.61	0.59	0.61	0.64
Σ interlayer charge	0.64	0.64	0.64	0.63	0.64	0.63	0.62	0.63	0.66
% tet. charge	0	0	3	7	5	9	1	0	1

	R7 300 525	R7 300 545	R7 300 580	R7 300 615	R7 300 650	R7 315 695	R7 315 765	R7 315 790	R7 R
Si	7.97	8.00	7.98	7.98	7.99	7.97	7.98	7.99	8.00
Al	0.03	0.00	0.02	0.02	0.01	0.03	0.02	0.01	0.00
Σ tet	8.00	8.00	8.00	8.00	8.00	8.00	8.00	8.00	8.00
Al	3.10	3.08	3.09	3.09	3.09	3.09	3.09	3.10	3.10
Ti	0.01	0.01	0.01	0.01	0.01	0.01	0.01	0.01	0.01
Fe3+	0.36	0.37	0.36	0.36	0.36	0.37	0.36	0.36	0.36
Mg	0.48	0.49	0.49	0.49	0.48	0.49	0.49	0.47	0.47
Σ oct	3.96	3.95	3.95	3.95	3.94	3.95	3.95	3.94	3.93
Ca	0.01	0.02	0.01	0.02	0.02	0.02	0.01	0.02	0.01
Na	0.61	0.61	0.62	0.61	0.62	0.62	0.63	0.61	0.63
Σ interlayer charge	0.63	0.65	0.64	0.65	0.66	0.65	0.65	0.65	0.65
% tet. charge	5	1	4	4	1	5	4	1	0

The chemical data for the < 1 µm fraction have also been used for calculations of the average structural formula of the smectite. The following assumptions and simplifications were made in these calculations:

1. All structural **iron** was assumed to be trivalent although no determination was made of the oxidation state. The assumption that all octahedral iron is present only in the ferric state may underestimate the octahedral charge.
2. **Calcium** has been assigned to the pool of interlayer cations because any calcium carbonate/sulphate that survived the pre-treatments will dissolve during the dialysis, supplying calcium for exchange. The same would be true for magnesium but no soluble Mg-bearing phase has been identified.
3. **Magnesium** was assigned to the octahedral sheet since the clay was saturated with sodium and dialyzed prior to the chemical analysis in order to make the allocation of cations to exchange and structural sites, respectively, less ambiguous. The interlayer charge would be underestimated if some of the magnesium found by chemical analysis of the fine clay is exchangeable.

4. All **potassium** (range 0.06–0.09% K_2O) was allocated to illitic layers in the smectite structure since no discrete potassium-bearing minerals were detectable in any of the XRD-profiles of the < 1 μm fractions. The proportion of illite was calculated assuming the average K_2O-content of illite to be 8.5% (cf. Newman and Brown 1987); the SiO_2 and Al_2O_3 contents were adjusted accordingly.
5. All remaining **silica** was allocated to the tetrahedral sheet of the smectite although the XRD-data indicate that traces of very fine-grained cristoballite may still exist in the purified fine-clay fractions. A "contamination" of the smectite with free silica would decrease the calculated tetrahedral charge.

The structural formulas of the smectite are presented in Table 3-7. No clear trends can be seen in the average crystal chemistry, neither within nor between the blocks and those variations that exist are within the accuracy of the method. Accordingly, the resulting average formulas (per $-O_{10}(OH)_2$ formula unit) of the montmorillonite of the blocks and the references are more or less identical:

References: $Ca_{0.01}\ Na_{0.32}\ Al_{1.55}\ Fe_{0.18}\ Mg_{0.24}\ Ti_{0.005}\ Si_{3.998}\ Al_{0.002}\ O_{10}(OH)_2$

Block C4: $Ca_{0.01}\ Na_{0.31}\ Al_{1.55}\ Fe_{0.18}\ Mg_{0.25}\ Ti_{0.005}\ Si_{3.99}\ Al_{0.01}\ O_{10}(OH)_2$

Block R7: $Ca_{0.01}\ Na_{0.31}\ Al_{1.55}\ Fe_{0.18}\ Mg_{0.24}\ Ti_{0.005}\ Si_{3.99}\ Al_{0.01}\ O_{10}(OH)_2$

3.2.6 X-ray diffraction analysis

The XRD-profiles of random powders of the reference samples are shown in Figure 3-9. The strongest peaks of the major non-phyllosilicates quartz, cristobalite and feldspars (K-and Na-feldspar), are indicated in the profiles. Traces of gypsum are generally found in MX-80 bentonite and the position of the strongest peak of gypsum is indicated in the figure, but according to the chemical data the maximum amount of gypsum that can exist (i.e. if all sulphur is allocated to $CaSO_4 \cdot 2H_2O$) in the reference bentonite is about 1.5% and close to the detection limit of the XRD analysis. Also calcite has been found in MX-80 (e.g. Karnland et al. 2000), and is indicated in the chemical data but, again, the quantity (~ 1.0% if all acid-soluble carbon is allocated to $CaCO_3$) is close to the detection limit.

Micaceous minerals have their (001) reflection at 10 Å, but occur in such small quantities that basal reflections can barely be detected in the XRD-trace of a randomly oriented preparation of good quality, but, depending on their degree of accidental orientation, individual samples may display a peak of low intensity in the 10 Å-region.

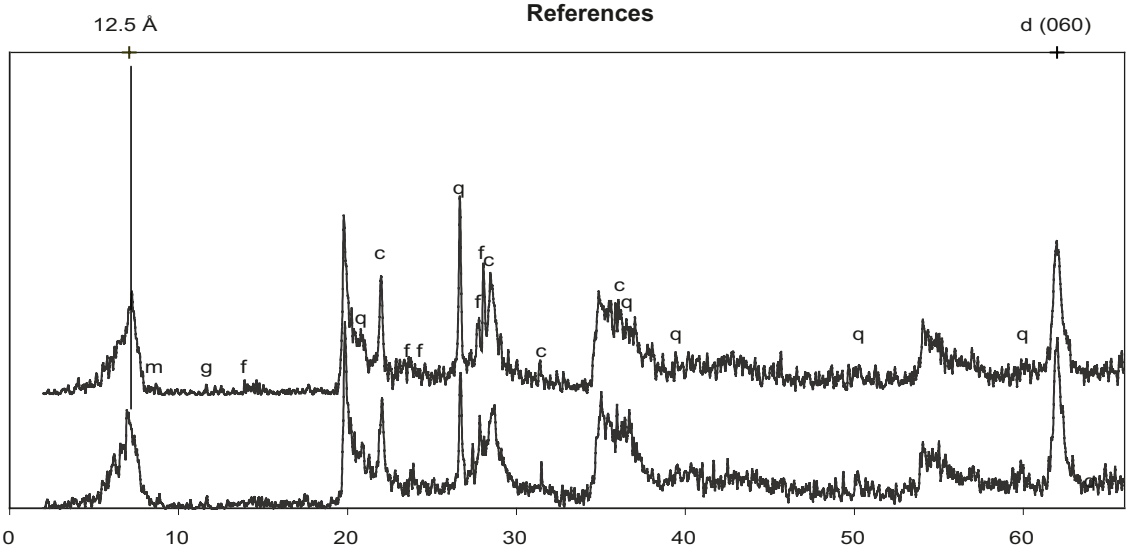

Figure 3-9. *XRD-profiles of random powders of the reference samples for block C4 and R7 of the CRT buffer. The position of the strongest peaks of the major accessory minerals is indicated: c = cristobalite; f = feldspars; g = gypsum, m = mica/illite q = quartz. The positions of the (001)-peak and the strongest hk-band (060) of montmorillonite are also indicated. CuKα radiation.*

In Figure 3-9 also the first order basal reflection of montmorillonite is indicated. The reference samples have a d-value of approximately 12.5 Å typical of the monolayer hydrate of Na-montmorillonite, which is stable at relative humidities below 60–70% (Brindley and Brown 1980). The shoulder on the low-angle side of the peak suggests, however, that mixed hydration states occur, probably due to the mixed interlayer cation pool of the bentonite – approximately 30% of the interlayer sites are occupied by divalent cations which form two-layer hydrates at the relative humidity of normal laboratory conditions.

In Figure 3-9 also the position of the two-dimensional hk-band d(060)-peak is indicated. This reflection is useful for recognizing di- and trioctahedral sub-groups of clay minerals since it includes the *b* cell dimension, which is sensitive to the size of the cations and to site occupancy in the octahedral sheet. An indicated d(060) value of 1.49–1.50 Å (62° 2θ) is typical of the dioctahedral sub-group of smectites, to which montmorillonite belongs.

The XRD-profiles of the bulk samples from the cool block C4 (Figure 3-10 top) display no significant changes compared with the reference samples, neither with respect to the type nor to the peak intensities of accessory minerals. A variation of the intensity of the feldspar peaks can be seen among the samples, but both the excellent {010} and {001} cleavage of feldspars, which promotes preferred orientation, and the coarse grain size of feldspars, may give a random variation in the peak intensities. Similarly, depending on the degree of random orientation of the preparation, some but not all samples display a 10 Å peak of low intensity produced by mica/illite.

The shape and width of the (001) basal reflection of montmorillonite varies somewhat among the samples but, like the references, all samples have the peak centered on 12.5 Å, which is typical of the monolayer hydrate of Na-montmorillonite and consistent with the data on the composition of the exchangeable cation pool, showing that the proportion between divalent and monovalent cations has changed very little compared with the reference bentonite.

The most conspicuous mineralogical change in the heated block R7 (Figure 3-10 bottom) is the appearance of moderately intense peaks of anhydrite ($CaSO_4$) in the contact sample. Accordingly, the mineralogical data match the chemical data, which show that Ca-sulphate has accumulated at the canister in block R7.

A close-up of the region 60–64° 2θ of the XRD-profiles of the buffer and reference samples (Figure 3-11) shows that the d-value of the (060) peak is more or less identical in all samples (~ 1.50 Å). Those variations that may exist appear to be random and independent of the position of the sample in the buffer. Thus, the available XRD-data provide no evidence of any significant change of the *b* cell dimension of the clay mineral, which would be an expected effect of, for instance, a change of the cations or the site occupancy in the octahedral sheet, or of a change of the amount of Al in tetrahedral coordination.

XRD-profiles of oriented mounts of the Mg-saturated, air-dried < 1 μm fraction of six of the samples from block R7 are shown in Figure 3-12. The basal spacing of the homo-ionic Mg-clay ranges from 14.7 to 15 Å (relative humidity 50±10%). Those variations that may exist appear to be random and independent of the position of the sample in the block and are in some cases an effect of variations in preferred orientation. In Figure 3-12 also the position of the strongest peak of cristobalite (4.05 Å) is indicated. A peak of very low intensity at this position in all samples may indicate that traces of very fine-grained cristobalite still exist in the < 1 μm fraction.

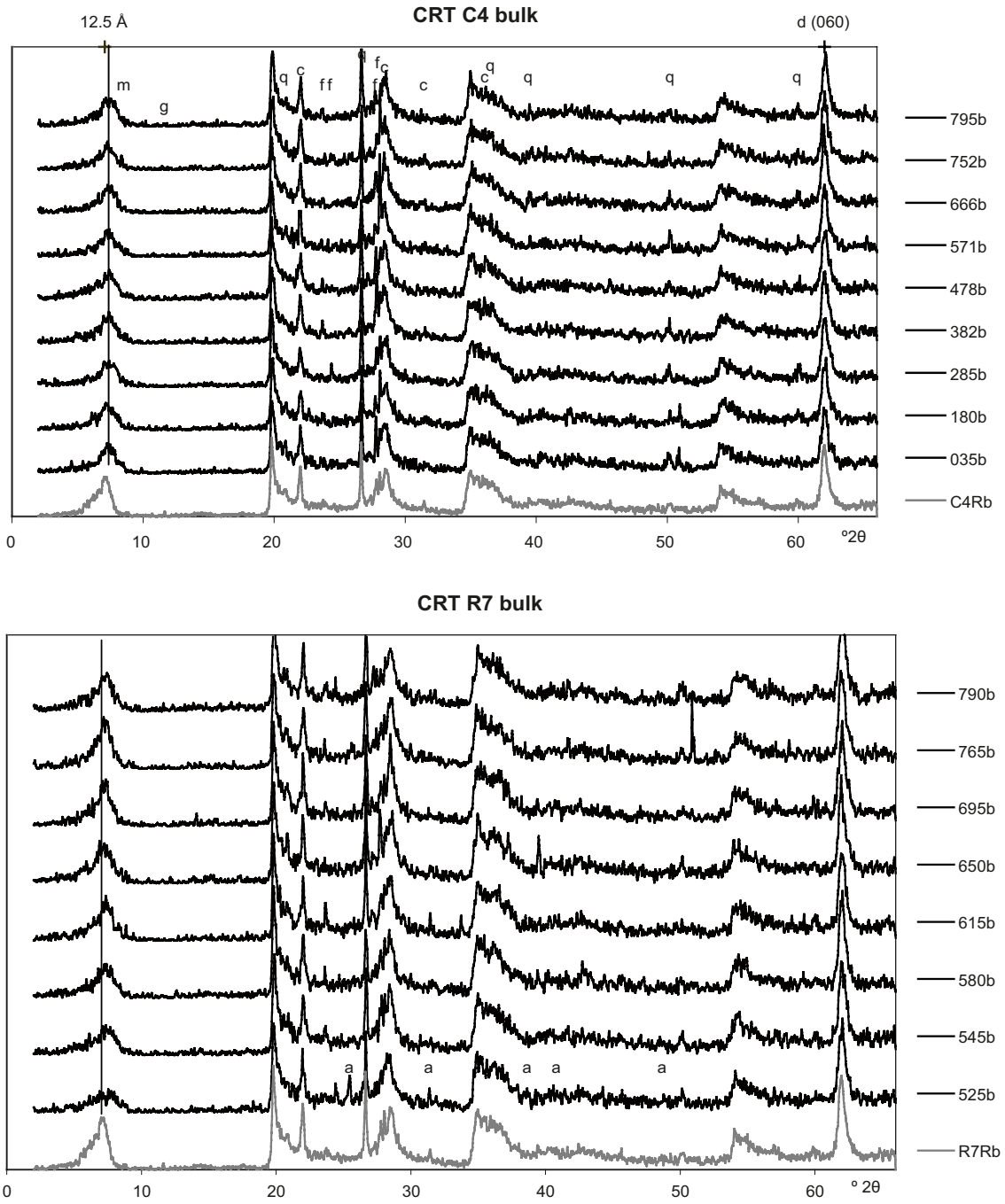

Figure 3-10. *Black curves: XRD-profiles of random powder of bulk samples from block C4 (top) and R7 (bottom) of the CRT buffer. Grey curves: XRD-profile of the reference sample. The position of the strongest peaks of the major non-clay minerals is indicated :a = anhydrite, c = cristobalite, f = feldspars, g = gypsum, q = quartz. The (001) peaks of mica/illite at 10 Å and of Na-smectite at 12.5 Å are also indicated. CuKα radiation.*

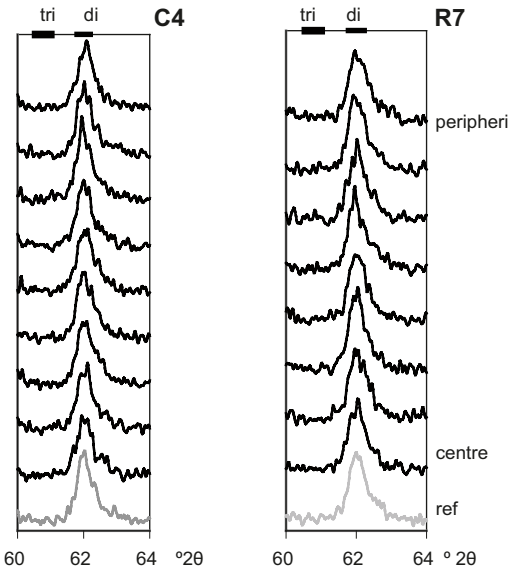

Figure 3-11. *Close-up of the (060)-peak position. Grey curve: XRD-profile of the reference samples. Radial positions for the samples are given in Figure 3-10. The indicated d-value (1.497 Å) of the (060)-peak is typical of dioctahedral smectites. The position of the (060)-peak of trioctahedral smectites is also indicated on the upper scale. Cu Kα radiation.*

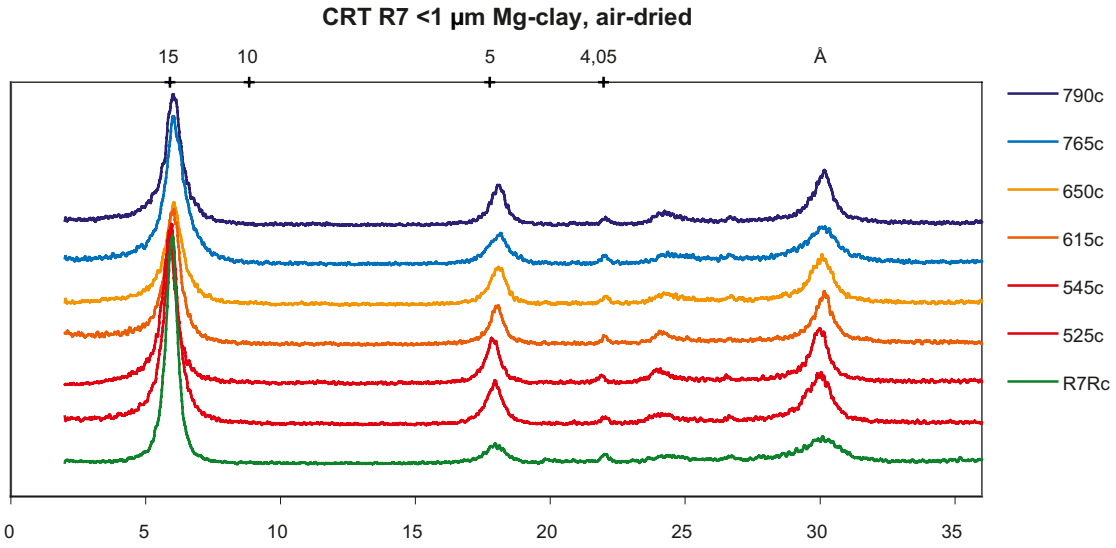

Figure 3-12. *XRD-profiles of oriented aggregates of the Mg-saturated, air-dried < 1µm fraction of six samples from block R7. Green curve: reference sample. The position of the strongest peaks of cristobalite (4.05 Å) and mica/illlite (10 Å) are indicated in the upper scale. CuKα radiation.*

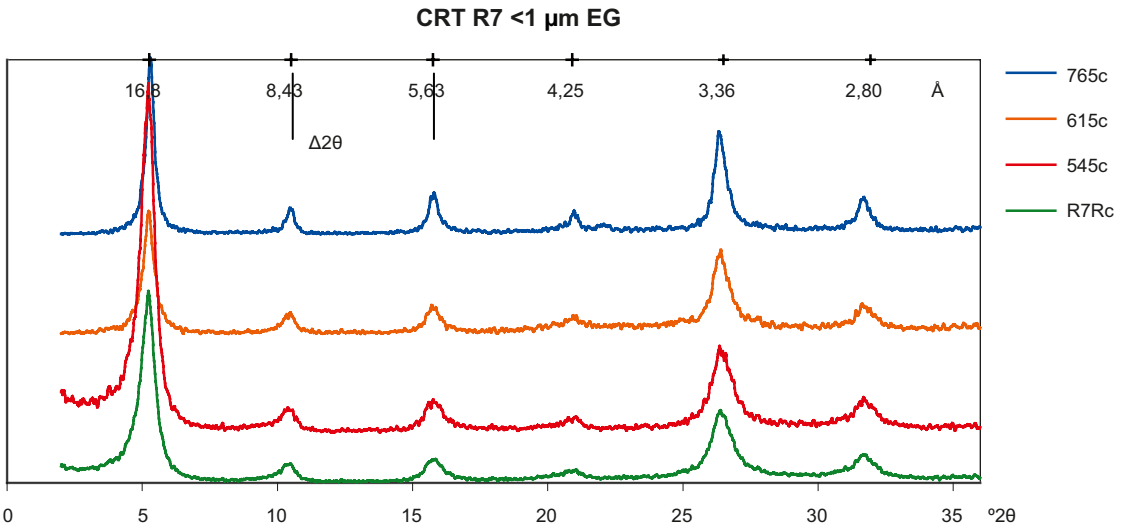

Figure 3-13. *XRD-profiles of oriented aggregates of the Mg-saturated, EG-solvated < 1µm fraction of three samples from block R7. Green curve: reference sample. The position of the basal reflections of montmorillonite is indicated in the upper scale. The value Δ2θ is explained in the text. CuKα radiation.*

The expansion behaviour was tested by EG-solvation of three of the samples from block R7, from a central, mid- and peripheral position (Figure 3-13).The expansion behavior of the smectite from the surface layer of block R7 could not be tested because the XRD-mount was curled, i.e. the orientation was destroyed, by the EG-solvation. This behavior is often seen in clays containing colloidal, organic matter, and might in this case be an effect of the oil-based contaminant in the sample. All the clay samples examined expand to 16.7–16.9 Å upon EG-solvation, which is typical of Mg-saturated montmorillonite. As can also be seen in the diffractograms of the EG-solvated clays, the series of basal reflections deviates little from a complete, periodic diffraction pattern, which is indicative of well-ordered stacking sequences with virtually no interstratification. Similarly, the value of $\Delta 2\theta_{002/003}$ (the angular difference between the (002) and (003) peaks in degrees 2θ) is in the same range (5.25–5.3) as that of the reference and typical of a well-defined montmorillonite phase (Moore and Reynolds 1989). Small amounts of non-exchangeable potassium in the < 1 µm fraction (0.06–0.09% K_2O) suggests that some illitic layers may exist in the smectite of all samples but in proportions (~1%) too small for detection by use of routine XRD analyses.

In summary, the available XRD-data provide no evidence of any structural change in the montmorillonite of the CRT buffer, but the resolution of the XRD-technique is inadequate for detecting subtle structural changes.

3.3 Conclusions

The chemical/mineralogical study of MX-80 bentonite subjected to heating and hydration by a natural Na-Ca-Cl-dominated groundwater in the 5 year-long, full-scale CRT experiment suggested that:

- under the thermal and hydration gradients that prevailed during the test period, calcium sulphate (anhydrite) accumulated at the canister in the heated part of the buffer,
- the equilibration of the exchangeable cation pool against the Na-Ca-dominated groundwater resulted in a small decrease in the proportion of exchangeable Mg in the peripheral parts of both blocks,
- Cu was incorporated into the bentonite matrix at the surface of the copper canister indicating some corrosion,
- the XRD characteristics, the cation exchange properties, and the average crystal chemistry of the Na-saturated fine clay fractions provided no evidence of chemical/structural changes in the montmorillonite.

4 Hydro-mechanical analyses

4.1 Swelling pressure and hydraulic conductivity tests

4.1.1 Material and methods

General

The hydraulic conductivity and swelling pressure of the buffer material are essential properties of the buffer material in a repository. These properties are among other factors affected by the method of measuring and under what conditions the measurements are made (Dixon et al. 1999). Furthermore the properties are functions of the density of the sample and the chemical composition of the water and the buffer material (Börgesson et al. 1995, Dixon et al. 1999, Karnland et al. 2006, 2009)

Equipment

The hydraulic conductivity and swelling pressure tests were made in oedometers with a diameter of 50 mm. The height of the samples was 20 mm (Figure 4-1). The specimens were saturated from the two filters placed at the bottom and top of the samples. A piston was placed on top of the specimen in order to keep its volume constant and the swelling pressure was continuously monitored using a load cell installed at the top of the cell. All the specimens were saturated and tested with groundwater from the test site.

Preparation of specimen and test procedure

Twelve tests were performed on trimmed specimens from block C4 and R7. Another six tests were made on material taken from the field experiment which was air dried and crushed to a grain size similar to MX-80 and compacted into the test cells to dry densities of about 1,550 kg/m^3, which after saturation of the specimen, corresponded to a density at saturation of about 2,000 kg/m^3, i.e. the reference density of the buffer for the KBS-3 concept. In addition, six reference tests were made on the same bentonite used in the manufacturing of the buffer blocks. These specimens were compacted into the test cells to dry densities between 1,310 and 1,580 kg/m^3 in order to cover the expected density range in the field experiment.

After saturation, a pore pressure gradient was applied across the specimen and the volume of the out-flowing water measured until stable rate of flow was established. The hydraulic conductivity was then calculated according to Darcy's law. The hydraulic gradient during the tests varied between 3,750–7,500 m/m (corresponding to a pore pressure difference across the sample of P_w = 750–1,500 kPa). No backpressure was used, i.e. the pore pressure on the outlet side was atmospheric. The measurements of the outflow were made over a period of several days in order to get stable flow values.

The water content and density were determined for each specimen after testing. The water content was determined as the ratio of the mass of water to the dry mass where the dry mass was determined after drying at 105°C for 24h (see Appendix 2). The bulk density was calculated from the total mass

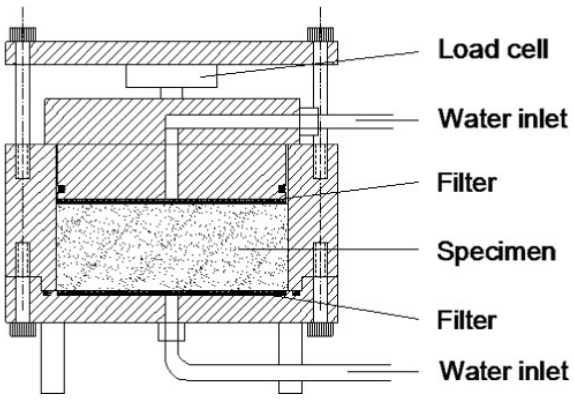

Figure 4-1. *A schematic drawing of an oedometer.*

of a sample and the volume determined by weighing the sample above and submerged in paraffin oil. From the determined water content and bulk density the degree of saturation was determined according to the procedure provided in Appendix 2.

4.1.2 Results

The results from the measurements of the swelling pressure and the hydraulic conductivity (Table 4-1) are plotted as a function of dry density (Figure 4-2). The values of the evaluated hydraulic conductivities in Figure 4-2 and Table 4-1 are determined at a pore pressure difference across the samples of 1,500 kPa (except for sample No C4:4 which was determined at a pore pressure difference of 750 kPa). The dry density was calculated from the water content and density measured at the end of the testing following rapid dismantling of the oedometer. The results are plotted together with the best fit curve determined for the reference specimens. The data for the air-dried and crushed samples had a significant scatter, compared to the rest of the data set, especially regarding the hydraulic conductivity. The figure shows that the swelling pressures for the specimens taken from the field tests have the same magnitude as for the reference specimens. The hydraulic conductivity is somewhat lower in the specimens taken from the field experiment compared to the reference samples. The calculated degree of saturation was higher than 99% for all specimens (Table 4-1).

In order to establish that the hydraulic conductivities measured are for saturated materials and that the assumptions of Darcian flow are valid tests were done at two substantially different hydraulic pressure heads (750 and 1,500 kPa). The results, shown in Figure 4-3 confirm that the hydraulic conductivity determined for the materials is an intrinsic parameter and not a function of test technique.

Table 4-1 Results from the measurements of swelling pressure and hydraulic conductivity. The maximum temperatures (T_{max}) at field exposure are evaluated from Figure 2-3.

Block/No	Preparation	Radial position	T_{max}.	w	ρ_d	e	S_r	Swelling pressure	Hydr. cond.
		mm	°C		kg/m^3			kPa	m/s
R7:1	Reference test			0.329	1,450	0.917	0.998	3,930	1.13E–13
R7:2	Reference test			0.287	1,550	0.796	1.002	5,700	7.72E–14
R7:3	Reference test			0.262	1,600	0.737	0.988	8,150	6.29E–14
C4:4	Reference test			0.406	1,310	1.115	1.013	1,620	1.86E–13
C4:5	Reference test			0.317	1,470	0.887	0.994	4,090	8.33E–14
C4:6	Reference test			0.273	1,580	0.759	1.000	8,720	5.12E–14
R7:7	air-dried	540	93	0.289	1,540	0.801	1.002	7,460	8.22E–14
R7:8	air-dried	580	88	0.292	1,540	0.808	1.004	6,170	9.93E–14
R7:9	air-dried	585	87	0.289	1,550	0.796	1.009	5,530	6.3E–14
R7:10	air-dried	665	78	0.284	1,550	0.797	0.990	5,570	7.7E–14
R7:11	air-dried	765	70	0.286	1,540	0.800	0.992	6,170	1.1E–13
C4:12	air-dried	35	25	0.285	1,550	0.798	0.993	6,580	6.9E–14
R7:13	trimmed	540	93	0.288	1,540	0.776	0.998	5,560	6.2E–14
R7:14	trimmed	560	90	0.282	1,550	0.780	0.992	5,150	5.7E–14
R7:15	trimmed	580	88	0.286	1,550	0.777	0.995	4,970	5.7E–14
R7:16	trimmed	600	85	0.291	1,540	0.774	1.006	4,730	6.7E–14
R7:17	trimmed	585	87	0.268	1,590	0.788	0.999	7,960	3.7E–14
R7:18	trimmed	605	85	0.286	1,560	0.787	1.012	6,370	4.9E–14
R7:19	trimmed	665	78	0.259	1,610	0.723	0.996	9,020	3.3E–14
R7:20	trimmed	695	76	0.265	1,590	0.748	0.984	7,510	3.6E–14
R7:21	trimmed	765	70	0.274	1,570	0.770	0.989	6,260	4.1E–14
R7:22	trimmed	790	68	0.268	1,590	0.750	0.992	9,290	3.4E–14
C4:23	trimmed	35	25	0.273	1,570	0.767	0.990	7,100	5.2E–14
C4:24	trimmed	752	25	0.279	1,560	0.782	0.994	5,970	5.3E–14

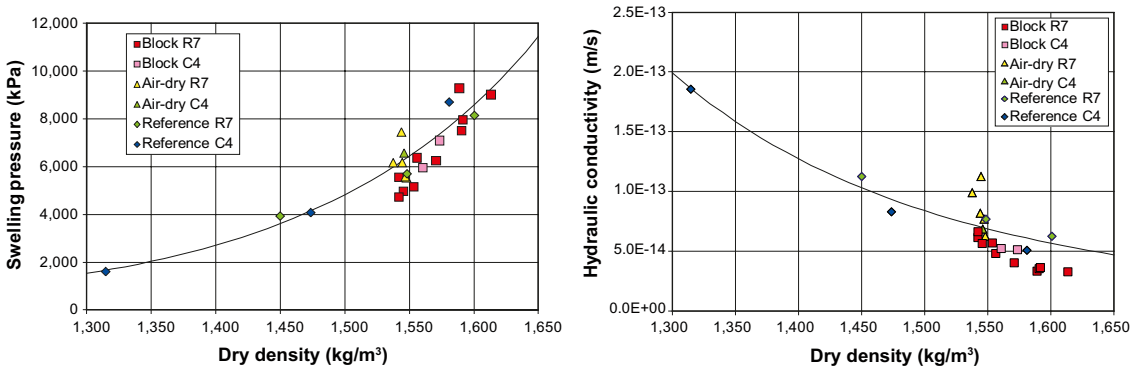

Figure 4-2. *The determined swelling pressure (left) and hydraulic conductivity as function of the dry density of the samples (right).*

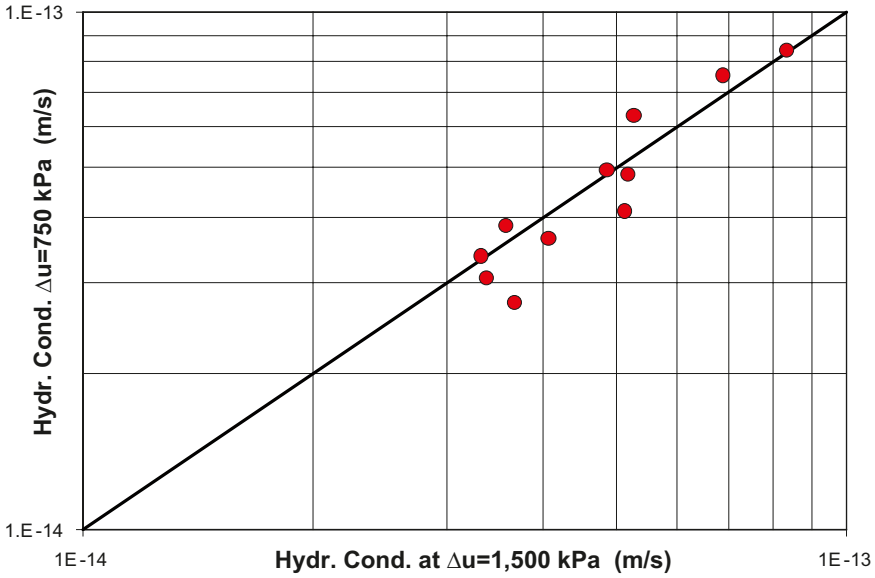

Figure 4-3. *Evaluated hydraulic conductivity in the 11 samples at a Δu of 750 kPa as function of the hydraulic conductivity at a Δu of 1,500 kPa.*

The measured hydraulic conductivities for the specimens taken from the field test deviate from the reference tests at higher densities by up to a factor of two (Figure 4-2 right). This might be an effect of the position of the specimens in the buffer and thus the maximum temperature they have been exposed to. The results from the measurements of the hydraulic conductivity for the specimens taken from block R7 are compared with the data from the reference specimens (Figure 4-4). The plot indicates that although the quantity of data is limited, that the location within the CRT has not substantively affected the hydraulic conductivity of the buffer. All of the data follow the same trend.

An attempt to further probe the dependence of hydraulic conductivity on dry density and maximum temperature from block R7 is established in Figure 4-5. It must however be understood that due to the limited amount of data, the analysis only indicates the qualitative property of the dependencies. Three samples have been identified as being at "constant temperature", in the range of 85–87°C, and three samples as being at "constant density", in the range of 1,589–1,591 kg/m^3 (Figure 4-5, left). Straight lines fitted against the "constant temperature" and "constant density" samples in the planes of dry density – hydraulic conductivity and temperature – hydraulic conductivity, respectively, indicate the strength of the dependence (Figure 5-5, mid and right). This analysis shows no clear effect of temperature on the hydraulic conductivity of these materials and the usual density-hydraulic conductivity relationship is observed.

The swelling pressures and hydraulic conductivities measured in the CRT are consistent with those reported for a field test with similar design to the CRT but of smaller scale and with higher operating temperature and steeper temperature gradient (Karnland et al. 2009).

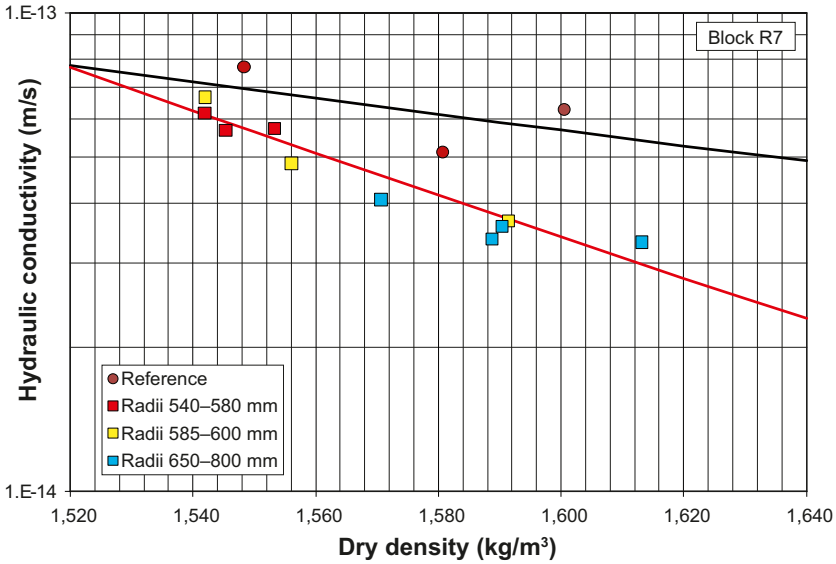

Figure 4-4. *A detail plot of the hydraulic conductivity determined on samples taken from block R7 together with the results from the reference specimens.*

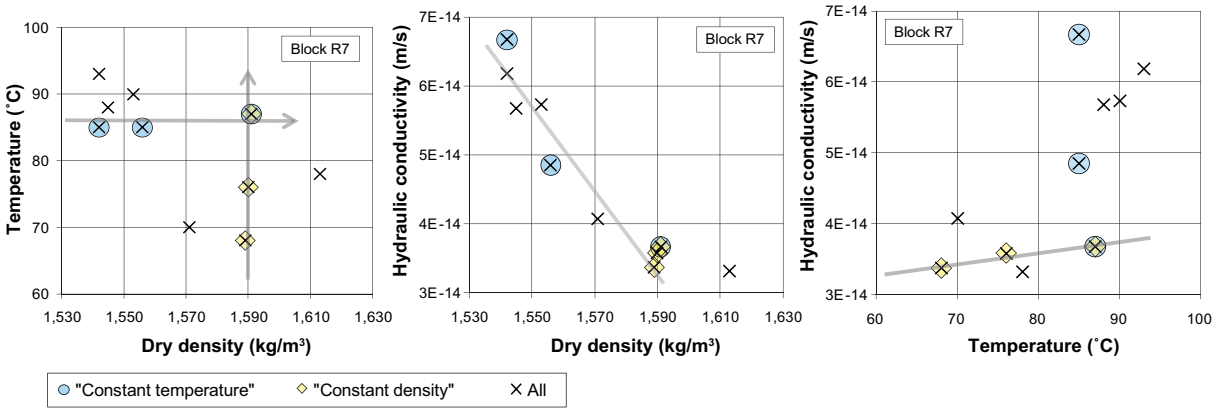

Figure 4-5. *Graphical representations of dry density, maximum temperature and hydraulic conductivity for samples from block R7. Temperature vs. dry density (left), where the horizontal and vertical arrows indicate the motivation of the sample categories "constant temperature" and "constant density", respectively. Hydraulic conductivity vs. dry density (mid), where the line schematically indicates the dry density dependence. Hydraulic conductivity vs. temperature (right), where the line schematically indicates the temperature dependence.*

4.1.3 Conclusions

The following conclusions were drawn from the tests made for determining the hydraulic conductivity and swelling pressure:

- the swelling pressure of the field test material was in the same range as that of the reference material,
- the swelling pressure and the hydraulic conductivity of the field test material were independent of the position of the specimens in the field test and the maximum temperature they had been exposed to,
- although the data were limited, measurements at different pore pressure gradient indicated that the evaluated hydraulic conductivity was not affected by the pore pressure gradient,
- the hydraulic conductivity of the trimmed specimens taken from the field experiment was somewhat lower than that of the reference tests, especially at higher densities.

The conclusions above imply that the five years of field exposure of the bentonite has only affected the swelling pressure and the hydraulic conductivity to a minor extent.

4.2 Unconfined compression test

4.2.1 Material and method

General

The unconfined compression test method was used in several studies by Börgesson et al. (2003), Dueck (2010), Dueck et al. (2010), and Karnland et al. (2009) where the mechanical properties of bentonite were of interest. The unconfined compression test is an experimentally simple method where a cylindrical specimen is compressed axially under a constant rate of strain with no radial confinement or external radial stress.

Test series

Two types of specimens were prepared for testing, a tall type (40 mm) used for determination of shear strength and a short type (20 mm) used for comparison of mechanical behavior between specimens taken from different positions and reference specimens. The shear strength is commonly determined on specimens with a height equal to double the size of the diameter (H=2D) to allow the shear failure to fully develop without boundary effects from the end surfaces. The short type of specimens had heights equal to diameters (H=D), and the end effect was minimized by lubrication of the end surfaces. The diameter of the specimens was kept at 20 mm in order to optimize the spatial resolution across the profile of the field experiment.

The tall specimens (series CRTUCS) were drilled from blocks R7 and C4 from the field experiment (CRTUCS01 to CRTUCS12) or compacted from reference material (CRTUCS13 to CRTUCS15 and CRTUCS101). The twelve specimens from the buffer material were drilled from six different positions. From each position two different specimens were prepared in two slightly different ways, one was saturated after drilling and one was not.

The short specimens (series CRTUC) were drilled from cylinder C4 (CRTUC01 to CRTUC03), from ring R7 (CRTUC04 to CRTUC12, CRTUC19 to CRTUC24, CRTUC101 to CRTUC110 and CRTUC114 to CRTUC120) or compacted from reference material (CRTUC13 to CRTUC18, CRTUC111 to CRTUC113 and CRTUC121 to CRTUC124).

The field exposed material was retrieved as large sectors or as core samples with a diameter of 50 mm, cf. Section 2.4. From ring R7 the large sectors and the core samples were taken from the horizontal angles 300° and 315°, respectively, given in the labels of each sample. All specimens from block C4 were retrieved as cores.

Equipment

Most of the specimens were saturated in a custom designed steel device before the shear test. The short specimens aimed at studying relative changes were then placed in a mechanical press according to the set-up in Figure 4-6 where a constant rate of strain was applied to the specimens. The end surfaces were lubricated to minimize the end effects of the specimens. The same mechanical press was used for the tall specimens aimed at measuring shear strength, Figure 4-7. During both tests the deformation and the applied force were measured by means of a load cell and a deformation transducer. All transducers were calibrated prior to the shearing of one series and checked afterwards.

Preparation of specimens

Cylindrical specimens were prepared for all tests but different preparation techniques were used based on the methods needed to prepare the source materials for testing. The specimens were either prepared on material from the field experiment by drilling and trimming or prepared from powder in a compaction device. All specimens were prepared to the same dimensions; 20 mm in diameter and 20 mm in height.

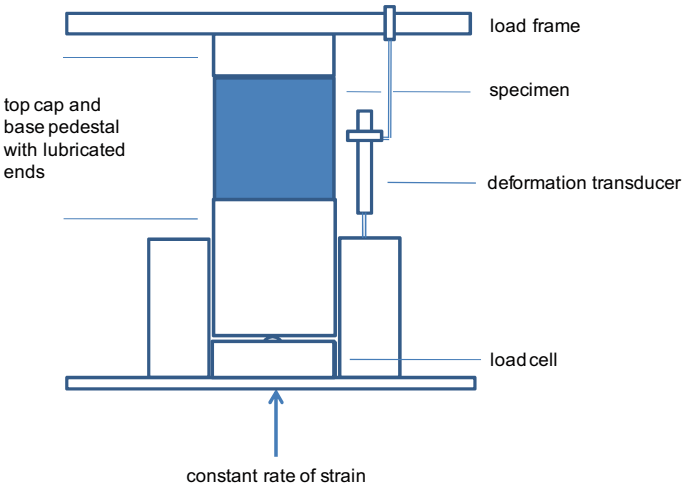

Figure 4-6. *Set-up for the unconfined compression test on short specimens.*

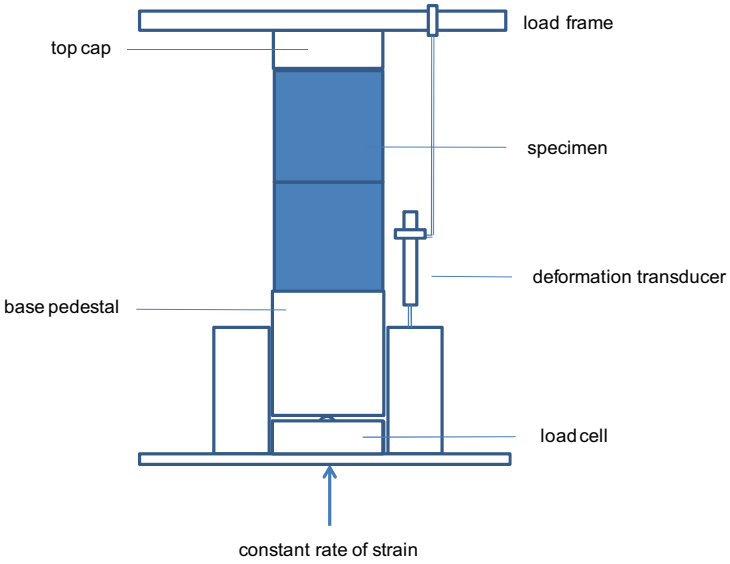

Figure 4-7. *Set-up for the unconfined compression test on tall specimens.*

The CRT field experiment was excavated in 2006. The main part of the samples for the unconfined compression tests were prepared one year later but supplementary samples were prepared four years later. To restore the conditions as much as possible all specimens except six tall specimens (CRTUCS07-CRTUCS12) were saturated before shearing.

The saturation was done in a special device during 2 weeks with groundwater from the test site, after evacuation of air from the filters and tubes. The specimens were removed from the saturation device at least 12 h before the shearing tests to homogenize, while protected against evaporation. In order to reduce the saturation time for the tall specimens, two short specimens were used and placed on top of each other at shearing.

Test procedure

The specimens were placed in the mechanical press (Figure 4-6 or Figure 4-7) and the compression was run at a constant strain rate of 0.8%/min which corresponds to 0.16 mm/min for the short specimens and 0.32 mm/min for the tall specimens. During compression the specimens were surrounded by a thin plastic film to minimize evaporation of water but did not affect pore pressure conditions within the specimens. After failure the water content and density were determined according to Appendix 2.

Evaluated variables

The specimens were considered as undrained during shearing and no volume change was taken into account. The deviator stress q (kPa) and the strain ε (%) were derived from Equation 4-1 and Equation 4-2, respectively, and calculated from the applied vertical load F, the original cross section area A_0, the initial length l_0, and the change in length Δl.

$$q = \frac{F}{A_0} \cdot \left(\frac{l_0 - \Delta l}{l_0}\right) \tag{4-1}$$

$$\varepsilon = \frac{\Delta l}{l_0} \tag{4-2}$$

The results were corrected for initially slightly uneven contact surfaces. This was done by decreasing the strain with the intercept on the x-axis of the tangent to the stress-strain curve taken at 500 kPa. The new starting point is illustrated in Figure 4-8.

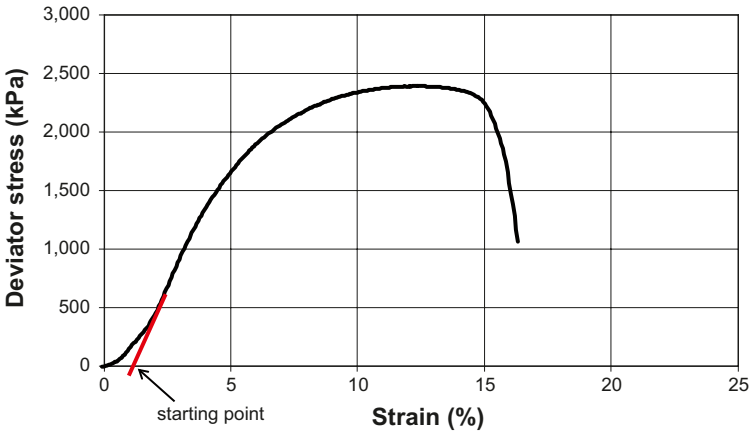

Figure 4-8. *Illustration of the starting point after correction for initially slightly uneven contact surface.*

4.2.2 Results

All results from the test series on short (CRTUC) and tall (CRTUCS) specimens are shown in Table 4-2 and 4-3.

Table 4-2. Results from test Series CRTUC with short specimens (H=D). All specimens were saturated with groundwater from the CRT test site. Duplicated specimen are denoted by the suffix d. Final dry density (ρ_d), final water content (w), final degree of saturation (S_r), maximum deviator stress (q_{max}), strain at q_{max} (ε), and maximum temperature during the field experiment according to Figure 2-3 (T_{max}).

Test ID	Material (Block:Angle: Radial distance)	ρ_d kg/m^3	w %	S_r %	q_{max} kPa	ε %	T_{max} °C	Remarks
CRTUC01	C4:225:035	1,540	28.8	99	2,210	12.0	28	
CRTUC02	C4:225:752	1,500	30.0	98	1,880	10.4	28	
CRTUC03	C4:315:795	1,530	29.1	99	2,220	10.8	28	
CRTUC04	R7:300:540	1,600	26.2	99	2,180	4.2	93	pronounced crack
CRTUC05	R7:300:575	1,580	27.2	99	2,630	9.2	87	
CRTUC05d	R7:300:560	1,520	29.8	99	1,890	10.1	89	slight crack
CRTUC06	R7:300:605	1,590	27.0	100	2,710	8.9	84	
CRTUC07	R7:315:585	1,600	26.2	99	3,000	8.2	86	
CRTUC07d	R7:315:585	1,550	28.6	100	2,220	9.4	86	
CRTUC08	R7:315:605	1,600	26.8	100	2,800	8.1	84	
CRTUC08d	R7:315:605		27.3		2,450	7.1	84	
CRTUC09	R7:315:665	1,590	26.9	100	2,580	8.9[1]	79	
CRTUC10	R7:315:695	1,590	26.8	99	2,580	10.3[1]	77	
CRTUC11	R7:315:765	1,550	28.2	99	2,160	10.1[1]	70	
CRTUC12	R7:315:790	1,560	28.0	99	2,220	9.5[1]	68	
CRTUC13	C4R	1,330	38.9	99	650	10.7	20	
CRTUC14	C4R	1,470	31.7	99	1,550	10.2	20	
CRTUC15	C4R	1,580	27.0	99	2,580	8.8	20	
CRTUC15d	C4R	1,590	26.5	99	2,670	9.4[1]	20	
CRTUC16	R7R	1,340	38.1	99	720	10.3	20	
CRTUC17	R7R	1,460	32.4	100	1,480	9.7	20	
CRTUC18	R7R	1,570	27.2	99	2,530	8.9	20	
CRTUC19	R7:300:535	1,580	27.3	100	2,140	4.6	93	pronounced crack
CRTUC20	R7:300:580	1,600	25.9	98	2,890	7.2	86	
CRTUC21	R7:300:610	1,610	25.6	98	3,330	6.1	84	
CRTUC22	R7:300:645	1,600	26.2	99	3,000	7.2	81	
CRTUC23	R7:315:585	1,640	24.5	98	3,920	6.2	86	
CRTUC24	R7:315:605	1,630	24.9	98	3,580	6.6	84	
CRTUC101	R7:300:540	1,540	28.8	99	2,050	5.4	93	slight crack
CRTUC102	R7:300:545	1,520	29.8	100	1,890	6.5	92	
CRTUC103	R7:300:565	1,550	28.2	99	2,440	8.3	88	
CRTUC104	R7:300:590	1,550	28.6	101	2,370	5.4	86	
CRTUC105	R7:300:595	1,550	28.7	100	2,270	8.9	85	
CRTUC106	R7:300:625	1,560	28.4	100	2,310	9.0	83	
CRTUC107	R7:315:665	1,620	25.2	99	3,630	9.4	79	
CRTUC108	R7:315:695	1,630	25.0	99	3,790	8.7	77	
CRTUC109	R7:315:765	1,630	25.0	99	3,740	7.5	70	
CRTUC110	R7:315:790	1,600	26.4	99	3,070	11.0	68	
CRTUC111	R7R	1,330	39.1	99	690	12.1	20	
CRTUC112	R7R	1,450	32.8	99	1,570	12.6	20	
CRTUC113	R7R	1,540	28.4	98	2,390	11.4	20	
CRTUC114	R7:300:600	1,520	29.8	100	2,080	10.8	85	
CRTUC115	R7:300:570	1,520	29.6	99	2,080	11.1	88	
CRTUC116	R7:300:560	1,530	28.9	98	2,120	12.0	88	
CRTUC117	R7:300:5,3[2]	1,530	29.2	99	2,380	7.1	94	slight crack
CRTUC118	R7:300:5,3[2]	1,550	28.1	99	2,450	4.5	94	
CRTUC119	R7:300:5,3[2]	1,530	29.7	101	2,220	4.9	94	
CRTUC120	R7:300:5,3[2]	1,560	28.0	99	2,310	3.3	94	slight crack
CRTUC121	R7R	1,600	25.7	96	3,210	7.7	20	
CRTUC122	R7R	1,620	25.2	97	3,320	6.4	20	
CRTUC123	R7R	1,660	23.4	97	4,450	6.6	20	
CRTUC124	R7R	1,660	23.6	97	4,530	6.8	20	

[1] Corrected for less rigid set up; [2] Sampling perpendicular to the ordinary vertical sampling.

Table 4-3. Results from test Series CRTUCS with tall specimens (H=2D). All specimens except CRTUCS07 to UCS12 were saturated with groundwater from the CRT test site. Final dry density (ρ_d), final water content (w), final degree of saturation (S_r), maximum deviator stress (q_{max}), strain at q_{max} (ε), maximum temperature during the field experiment according to FIgure 2-3 (T_{max}).

Test ID	Material (Block:Angle: Radial distance)	ρ_d kg/m^3	w %	S_r %	q_{max} kPa	ε %	T_{max} °C	Remarks
CRTUCS01	C4:225:752	1,500	30.7	100	1,800	7.0	28	
CRTUCS02	R7:300:540	1,440	32.9	99	1,370	6.7	93	slight crack
CRTUCS03	R7:300:560	1,500	31.0	100	1,800	7.5	89	slight crack
CRTUCS04	R7:315:585	1,590	26.7	99	2,410	5.1[1]	85	
CRTUCS05	R7:315:665	1,580	27.1	100	2,430	6.2[1]	79	
CRTUCS06	R7:315:790	1,550	28.4	100	2,090	7.4[1]	68	
CRTUCS07	C4:225:752	1,740	17.2	80	7,090	2.3	28	
CRTUCS08	R7:300:540	1,650	23.9	97	770[2]	2.6[2]	93	slight crack
CRTUCS09	R7:300:565	1,640	24.2	96	2,480	1.9	88	slight crack
CRTUCS10	R7:300:600	1,650	24.0	97	4,450	4.0	83	
CRTUCS11	R7:300:635	1,650	24.2	98	4,610	4.1	82	
CRTUCS12	R7:315:790	1,760	19.0	91	9,870	3.0	68	
CRTUCS13	R7R	1,330	39.9	101	610	8.4	20	
CRTUCS14	R7R	1,460	32.3	100	1,450	8.6	20	
CRTUCS15	R7R	1,590	27.1	100	2,520	7.2	20	
CRTUCS101	R7R	1,660	23.6	97	4,480	5.7	20	

[1] Corrected for less rigid set-up; [2] Height equal to diameter H = D during shearing.

The specimens CRTUC09-12 and CRTUCS04-06 were unfortunately sheared with a less rigid set-up and a doublet of the reference tests CRTUC15 (CRTUC15d) was run to evaluate a correction. The correction was then used for the evaluated strains of the actual specimens, shown in Tables 4-2 and 4-3.

In the diagrams below the colors refer to the temperatures coupled to the positions of the CRT buffer given in Section 2.2. From the warmest to the coldest the colors red, orange, yellow, green, dark blue and purple represent the temperatures 93°C, 87°C, 83°C, 78°C, 74°C and 69°C valid in the middle of the intervals 525–550, 551–600, 601–650, 651–700, 701–750 and 751–800 mm, respectively of ring R7. Cylinder C4 was exposed to an average temperature of 28°C marked with light blue.

All results from the short specimens from ring R7 are shown as deviator stress versus strain in Figure 4-9, Figure 4-10, and Figure 4-11 where the results are shown in the dry density intervals 1,500–1,550 kg/m^3, 1,551–1,600 kg/m^3, and 1,601–1,650 kg/m^3, respectively. Results from the corresponding reference specimens are shown in Figure 4-12.

From the results on reference specimens in Figure 4-12 the influence of density is clearly seen i.e. the higher the density the higher the maximum deviator stress q_{max} and the smaller corresponding strain ε. The maximum deviator stress q_{max} and the corresponding strain ε from tests on short specimens from the field experiment were plotted as a function of dry density with best fit lines from the reference tests (Figure 4-13). The colors of the markers refer to the positions and the corresponding temperature in block R7 and C4 according to the previous diagrams. Two specimens fell apart during sampling, marked with arrows, and the results are not considered to represent the maximum deviator stress for the intact material from the field experiment. The results from these two specimens deviate the most from the reference line in Figure 4-13, left.

A reduction in strain at failure, i.e. less strain than the solid reference best fit line, was seen on all specimens from the innermost part, i.e. from the region experiencing highest temperatures. These specimens also showed almost vertical failure surfaces, as can be seen in the photographs provided in Appendix 1.

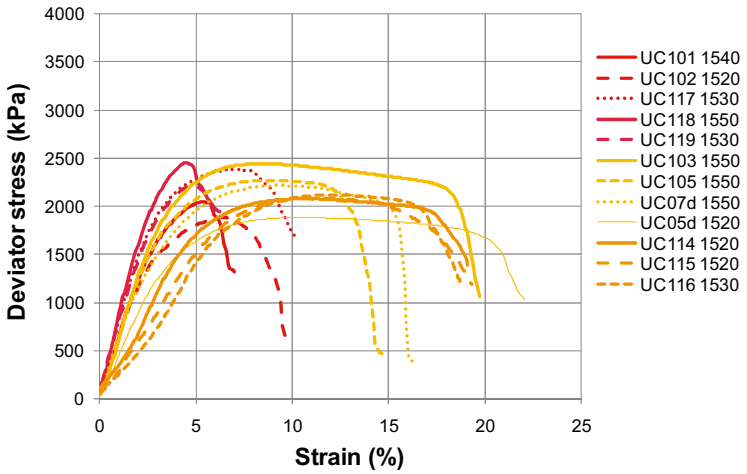

Figure 4-9. *Deviator stress versus strain on short specimens from ring R7 (Series CRTUC) in the dry density interval 1,500–1,550 kg/m^3. The colors red, orange, yellow, green, blue and purple represent distances from the canister and the temperatures 93°C, 87°C, 83°C, 78°C, 74°C and 69°C, respectively. The labels show the test ID and the dry density (kg/m^3).*

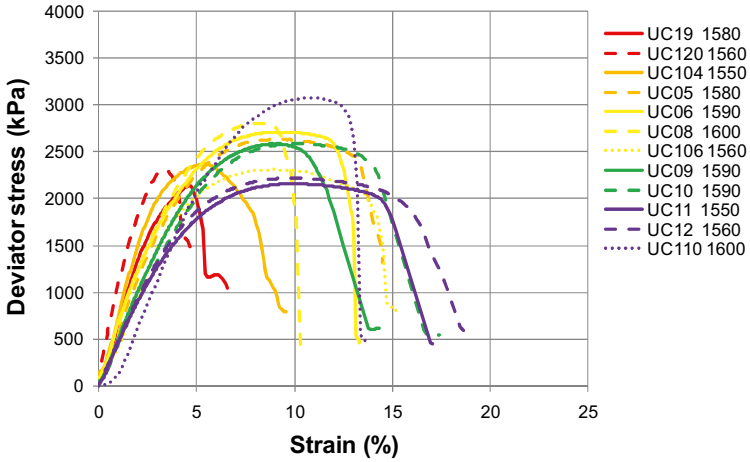

Figure 4-10. *Deviator stress versus strain on short specimens from ring R7 (Series CRTUC) in the dry density interval 1,551–1,600 kg/m^3. The colors red, orange, yellow, green, blue and purple represent distances from the canister and the temperatures 93°C, 87°C, 83°C, 78°C, 74°C and 69°C, respectively. The labels show test ID and dry density (kg/m^3).*

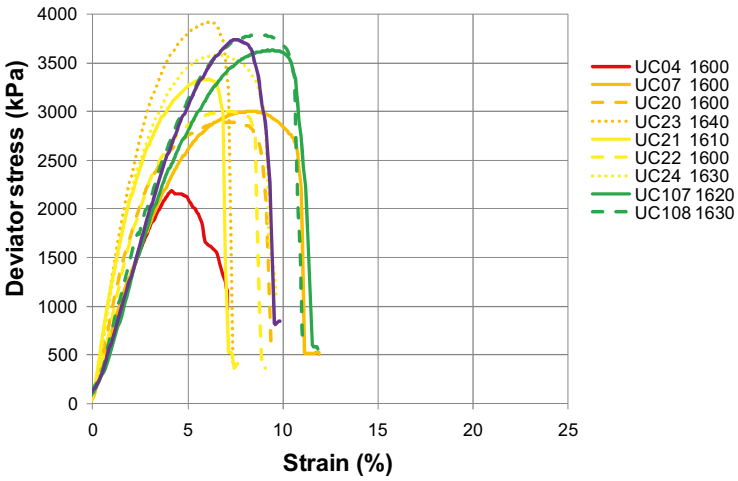

Figure 4-11. *Deviator stress versus strain on short specimens from ring R7 (Series CRTUC) in the dry density interval 1,601–1,650 kg/m³. The colors red, orange, yellow, green, blue and purple represent distances from the canister and the temperatures 93°C, 87°C, 83°C, 78°C, 74°C and 69°C, respectively. The labels show test ID and dry density (kg/m³).*

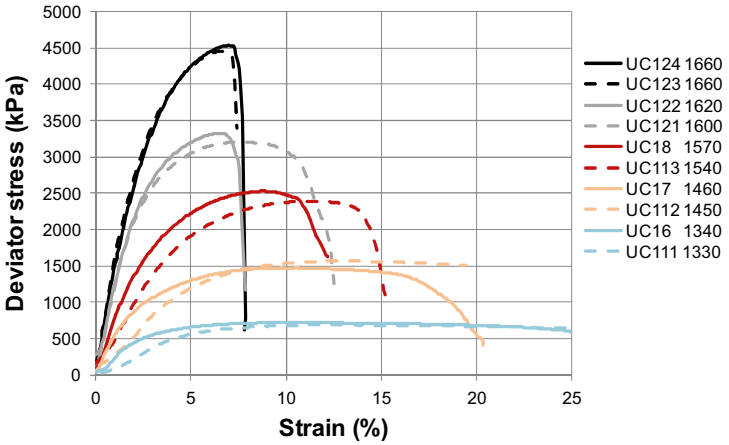

Figure 4-12. *Deviator stress versus strain on short specimens from reference material, R7R, (Series CRTUC). The labels show test ID and dry density (kg/m³).*

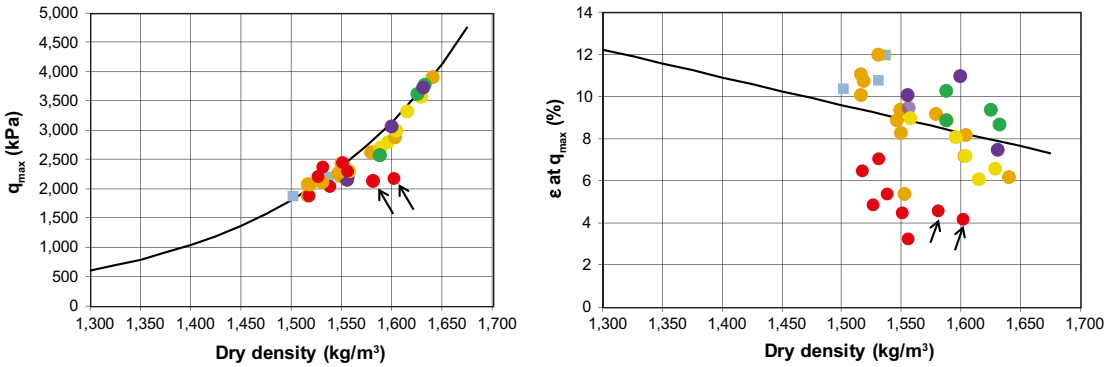

Figure 4-13. *Maximum deviator stress and strain versus dry density. Test results from the short specimens (series CRTUC) with the colors red, orange, yellow, green, dark blue, purple and light blue representing the temperatures 93°C, 87°C, 83°C, 78°C, 74°C, 69°C and 28°C, respectively. The trend-lines represent a best fit line from the reference tests.The arrows indicate specimens with a pronounced crack at sampling.*

The solid and dashed lines in Figure 4-14 represent best fit lines from reference tests on the short and tall specimens, respectively. The solid best fit lines are based on results shown with circles and squares and the dashed best fit lines are based on results shown with triangels. The circles and triangles represent the reference material R7R and the squares represent the reference material C4R. The same solid and dashed best fit lines are also shown in Figure 4-13 and Figure 4-15, respectively. In addition, the results from the short reference specimens of R7R (circles) were previously shown in Figure 4-12.

The shear strength, determined as the deviator stress at failure on the saturated tall type specimens, was plotted with the dashed best fit line from the reference tests and a dotted line representing a model for shear strength, also determined as the deviator stress at failure but based on triaxial tests on bentonite presented by Börgesson et al. (1995) (Figure 4-15, left). The strain at failure was also plotted with the dashed best fit line from the corresponding reference tests (Figure 4-15, right).

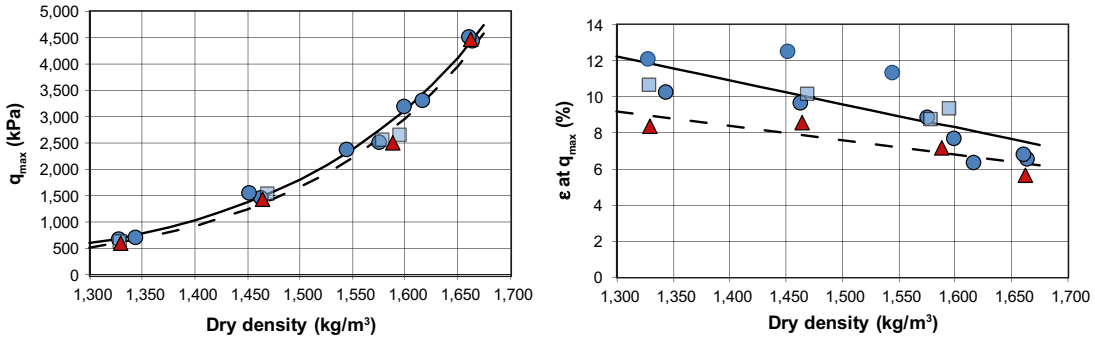

Figure 4-14. *Maximum deviator stress and strain versus dry density from all reference tests on short specimens (circles and squares) and tall specimens (triangles). The solid and dashed best fit lines for the short and the tall specimens, respectively are also shown.*

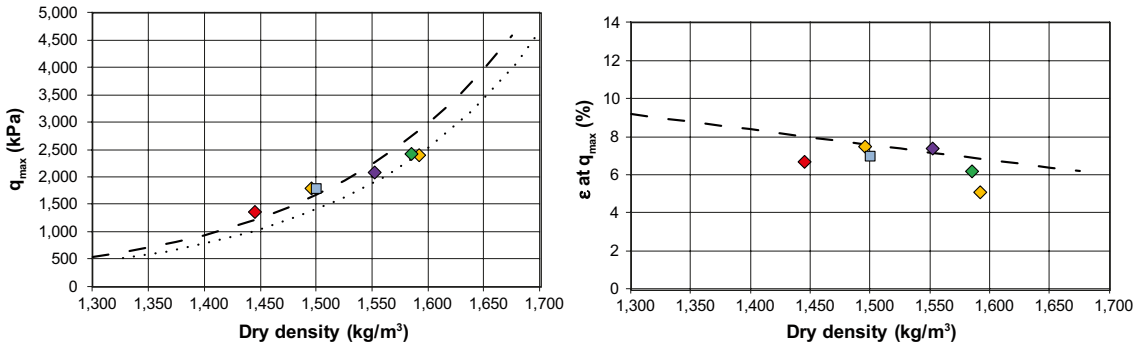

Figure 4-15. *Maximum deviator stress and strain versus dry density from the saturated tall specimens (CRTUCS). The dashed lines represent best fit lines from the reference tests and the dotted line represents a model presented by Börgesson et al. (1995).*

4.2.3 Discussion

From the results obtained from testing of short specimens a scatter was seen in the strain at failure, but a reduction of strain at failure was observed for all specimens taken from the innermost positions of block R7 compared to reference tests.

Regarding deviator stress at failure, with the exception of two specimens, there were no systematic deviations between the results obtained for the reference samples and the short ones. During preparation slight cracks were noticed on some of the innermost specimens and remarks were made in Tables 4-2 and 4-3. The two mentioned specimens had a more pronounced crack along the specimen but were saturated and sheared in spite of this, CRTUC04 and CRTUC19. Both specimens showed less maximum deviator stress and less strain than the references, however, the strain was in accordance with other specimens taken from the same positions. On some of the other specimens slight cracks were seen but, in contrast to the specimens with more pronounced cracks, no influence on the results could be observed. It is not possible to determine if the origin of the cracks was due to field exposure including heating, retrieval including decreases in temperature and stress, or the specimens being stored for a long time.

The reduction of strain at failure in the samples from the inner part of the buffer agreed with the results presented by Karnland et al. (2009) based on observations on specimens from a field experiment with comparable or higher temperatures. In the present study the reduction of strain at failure occurred at a position where accumulation of calcium sulfate was observed. In the comparable experiment (Karnland et al. 2009), a reduction of strain at failure was observed at positions with increased concentration of calcium sulfate but also at positions where no accumulation of calcium sulfate was seen. In the same study short-term laboratory heating tests were also performed, which also showed a reduction of strain at failure.

The shear strength evaluated as the deviator stress at failure from the re-saturated tall specimens agreed well with the references and slightly larger than the model of shear strength presented by Börgesson et al. (1995). That model was based on triaxial tests which were run at much lower strain rates than the unconfined compression tests which should give lower values of the strength (Dueck et al. 2010). The specimens which were not re-saturated, CRTUCS07 to CRTUCS12, are only presented in tabular form, i.e. in Table 4-3, since they were considered to have dried and shrunk and therefore not fully represent the material from the field experiment.

The reference tests in this study were run both on short and tall specimens. The maximum deviator stress resulting from the two types of specimens only differs slightly but the strain at failure was less for the tall specimens.

4.2.4 Conclusions

Based on this investigation, where properties of material exposed to repository-like conditions were compared to those of reference material, the following findings were found:

- a reduction of strain at failure was observed on re-saturated specimens from the innermost part, at a radial distance of 525–540 mm,
- no influence on deviator stress at failure was seen on re-saturated specimens of intact material from the field experiment,
- on some of the specimens with an observed and pronounced crack, a reduction of deviator stress at failure was noticed despite water re-saturation.

5 Summary and conclusions

The mineralogical stability of bentonite clays in different geological environments was one of the reasons for choosing bentonite as a buffer material in the Swedish KBS-3 concept for a repository for high-level radioactive waste. Nevertheless, alteration processes are expected to occur under the hydrothermal conditions that will prevail in the bentonite buffer. The present study of MX-80 bentonite subjected to heating at temperatures up to 95°C and hydration by a natural Na-Ca-Cl dominated groundwater in the 5 year-long, full-scaled experiment Canister Retrieval Test suggested that:

- under the thermal and hydration gradients that prevailed during the test period, calcium sulfate (anhydrite) accumulated near the canister in the heated part of the buffer,
- the equilibration of the exchangeable cation pool against the Na-Ca-dominated groundwater resulted in a small decrease in the proportion of exchangeable Mg in the peripheral parts of both blocks,
- at the surface of the copper canister, Cu was incorporated in the bentonite in a non-exchangeable, insoluble form,
- the crystal chemistry, the X-ray diffraction characteristics and the cation exchange properties of purified, Na-converted < 1 μm fractions provided no evidence of any structural changes in the montmorillonite,
- the swelling pressure of the field test material was in the same range as that of the reference material,
- the hydraulic conductivity of the trimmed specimens taken from the field experiment was somewhat lower than that of the reference tests, especially at higher densities,
- compared to the reference tests, a reduction of strain at failure was observed on re-saturated material taken close to the canister in the heated part of the buffer,
- no influence on deviator stress at failure was seen on re-saturated specimens of intact material from the field experiment compared to reference tests.

Whereas no structural alteration of the montmorillonite was detected, dissolution/precipitation and cation exchange reactions along with the water saturation under non-isothermal conditions resulted in small-scale chemical alterations of the bentonite.

Small changes were also observed in some of the THM properties of the bentonite retrieved from the field experiment. The exposure to high temperature may, in itself, have affected the mechanical properties of the bentonite, as demonstrated in previous short-term laboratory heating tests. The reduction of strain at failure, observed at positions close to the canister, may be related to anhydrite accumulation at this position. In contrast, no evident coupling was found between the somewhat lower hydraulic conductivity of the trimmed bentonite samples and their positions relative to the canister. This would argue that any redistributed mineral phases are not causing the small changes observed in the hydraulic behaviour of the buffer.

Based on this study the conditions imposed by the CRT's thermal and hydraulic evolution have not resulted in significant changes of the buffer properties.

References

SKB's (Svensk Kärnbränslehantering AB) publications can be found at www.skb.se/publications.

Abercrombie H J, Hutcheon I E, Bloch J D, de Caritat P, 1994. Silica activity and the smectite-illite reaction. Geology 22, 539–542.

Ammann L, Bergaya F, Lagaly G, 2005. Determination of the cation exchange capacity of clays with copper complexes revisited. Clay Minerals 40, 441–453.

Arcos D, Sena C, Salas J, 2010. Numerical modelling of the geochemical evolution of the near field under the hydrothermal conditions expected for a KBS-3 repository. In Clays in Natural and Engineered Barriers for Radioactive Waste Confinement: 4th International Meeting, Nantes, France, 29 March – 1 April 2010, 239–240.

Belyayeva N I, 1967. Rapid method for the simultaneous determination of the exchange capacity and content of exchangeable cations in solonetzic soils. Soviet Soil Science, 1409–1413.

Birgersson M, Karnland O, 2009. Ion equilibrium between montmorillonite interlayer space and an external solution – consequences for diffusional transport. Geochimica et Cosmochimica Acta 73, 1908–1923.

Brindley G W, Brown G (eds), 1980. Crystal structures of clay minerals and their x-ray identification. Mineralogical Society. Mon. No. 5. London.

Börgesson L, Johannesson L-E, Sandén T, Hernelind J, 1995. Modelling of the physical behaviour of water saturated clay barriers. Laboratory tests, material models and finite element application. SKB TR 95-20, Svensk Kärnbränslehantering AB.

Börgesson L, Johannesson L-E, Hernelind J, 2003. Earthquake induced rock shear through a deposition hole. Effect on the canister and the buffer. SKB TR-04-02, Svensk Kärnbränslehantering AB.

Dixon D A, Graham J, Gray M N, 1999. Hydraulic conductivity of clays in confined tests under low hydraulic gradients. Canadian Geotechnical Journal 36, 815–825.

Dixon D, Chandler N, Graham J, Gray M N, 2002. Two large-scale sealing tests conducted at Atomic Energy of Canada's underground research laboratory: the buffer-container experiment and the isothermal test. Canadian Geotechnical Journal 39, 503–518.

Dueck A, 2010. Thermo-mechanical cementation effects in bentonite investigated by unconfined compression tests. SKB TR-10-41, Svensk Kärnbränslehantering AB.

Dueck A, Börgesson L, Johannesson L-E, 2010. Stress strain relation of bentonite at undrained shear. Laboratory tests to investigate the influence of material composition and test technique. SKB TR-10-32, Svensk Kärnbränslehantering AB.

Dueck A, Johannesson L-E, Kristensson O, Olsson S, Sjöland A, 2011. Hydro-Mechanical and Chemical-Mineralogical analyses of the bentonite buffer from a full-scale field experiment simulating a high-level waste repository. Clay and Clay Minarals, Vol. 59, No. 6, 595–607.

Eberl D D, Velde B, McCormick T, 1993. Synthesis of illite-smectite from smectite at earth surface temperatures and high pH. Clay Minerals 28, 49–60.

Eng A, 2008. Äspö Hard Rock Laboratory. Canister retrieval test. Retrieval phase. Project report. SKB IPR-08-13, Svensk Kärnbränslehantering AB.

Fernández A M, Villar M V, 2010. Geochemical behaviour of a bentonite barrier in the laboratory after up to 8 years of heating and hydration. Applied Geochemistry 25, 809–824.

Gens A, Sánchez M, Guimarães L Do N, Alonso E E, Lloret A, Olivella S, Villar M V, Huertas F, 2009. A full-scale in situ heating test for high-level nuclear waste disposal: observations, analysis and interpretation. Géotechnique 59, 377–399.

Gómez-Espina R, Villar M V, 2010. Geochemical and mineralogical changes in compacted MX-80 bentonite submitted to heat and water gradients. Applied Clay Science 47, 400–408.

Goudarzi R, Börgesson L, Röshoff K, Edelman M, 2006. Äspö Hard Rock Laboratory. Canister retrieval test. Sensors data report (Period 001026–060501). Report No:12. SKB IPR-06-35, Svensk Kärnbränslehantering AB.

Hower J, Eslinger E V, Hower M E, Perry E A, 1976. Mechanism of burial metamorphism of argillaceous sediment: 1. Mineralogical and chemical evidence. Geological Society of America Bulletin 87, 725–737.

Huang W-L, Longo J M, Pevear D R, 1993. An experimentally derived kinetic model for smectite-to-illite conversion and its use as a geothermometer. Clays and Clay Minerals 41, 162–177.

Huertas F, Fariña P, Farias J, García-Siñériz J L, Villar M V, Fernández A M, Martín P L, Elorza F J, Gens A, Sánchez M, Lloret A, Samper J, Martínez M A, 2006. Full-scale engineered barriers experiment. Updated final report 1994–2004. Publicación Técnica 05-0/2006, ENRESA, Spain.

Jackson M L, 1975. Soil chemical analysis: advanced course. 2nd ed. Madison, WI: University of Wisconsin.

Johannesson L-E, 2007. Äspö Hard Rock Laboratory. Canister retrieval test. Dismantling and sampling of the buffer and determination of density and water ratio. SKB IPR-07-16, Svensk Kärnbränslehantering AB.

Karnland O, Birgersson M, 2006. Montmorillonite stablility. With special respect to KBS-3 conditions. SKB TR-06-11, Svensk Kärnbränslehantering AB.

Karnland O, Sandén T, Johannesson L-E, Eriksen T E, Jansson M, Wold S, Pedersen K, Motamedi M, Rosborg B, 2000. Long term test of buffer material. Final report on the pilot parcels. SKB TR-00-22, Svensk Kärnbränslehantering AB.

Karnland O, Olsson S, Nilsson U, 2006. Mineralogy and sealing properties of various bentonites and smectite-rich clay materials. SKB TR-06-30, Svensk Kärnbränslehantering AB.

Karnland O, Olsson S, Dueck A, Birgersson M, Nilsson U, Hernan-Håkansson T, Pedersen K, Nilsson S, Eriksen T E, Rosborg B, 2009. Long term test of buffer material at the Äspö Hard Rock Laboratory, LOT project. Final report on the A2 test parcel. SKB TR-09-29, Svensk Kärnbränslehantering AB.

Meier L P, Kahr G, 1999. Determination of the cation exchange capacity (CEC) of clay minerals using the complexes of copper(II) ion with triethylenetetramine and tetraethylenepentamine. Clays and Clay Minerals 47, 386–388.

Moore D M, Reynolds R C, 1989. X-ray diffraction and the identification and analysis of clay minerals. Oxford: Oxford University Press.

Newman A C D, Brown G, 1987. The chemical constitution of clays. In Newman A C D (ed). Chemistry of clays and clay minerals. Mineralogical Society. Mon. No. 6. New York: Wiley, 1–128.

SKB, 2011. Long-term safety for the final repository for spent nuclear fuel at Forsmark. Main report of the SR-Site project, Volume I. SKB TR-11-01, Svensk Kärnbränslehantering AB.

Thorsager P, Börgesson L, Johannesson L-E, Sandén T, 2002. Äspö Hard Rock Laboratory. Canister retrieval test. Report on installation. SKB IPR-02-30, Svensk Kärnbränslehantering AB.

Plötze M, Kahr G, Dohrmann R, Weber H, 2007. Hydro-mechanical, geochemical and mineralogical characteristics of the bentonite buffer in a heater experiment: the HE-B project at the Mont Terri Rock Laboratory. Physics and Chemistry of the Earth 32, 730–740.

Villar M V, Lloret A, 2007. Dismantling of the first section of the FEBEX in situ test: THM laboratory tests on the bentonite blocks retrieved. Physics and Chemistry of the Earth 32, 716–729.

Weaver C E, 1989. Clays, muds, and shales. Amsterdam: Elsevier. Developments in sedimentology 44.

Appendix 1

Unconfined compression tests

Vertical failure surfaces

Reduced strain at failure, less strain than the reference best fit line, was seen on all specimens from the innermost part, see Figure 4-13. These specimens also showed almost vertical failure surfaces, exemplified in Figure A1-1 below. Five reference specimens were tested in the actual dry density interval. Four of these showed ordinary failure surfaces according to Figure A1-2 and the fifth reference specimen showed something in between an ordinary and a vertical failure surface, Figure A1-3.

Figure A1-1. *Specimens CRTUC119 and CRTUC04 from the innermost part of the buffer with dry densities of 1,530 kg/m^3 and 1,600 kg/m^3, respectively.*

Figure A1-2. *Reference specimens CRTUC113 and CRTUC122 with dry densities 1,540 kg/m^3 and 1,620 kg/m^3, respectively.*

Figure A1-3. *Reference specimen CRTUC15 with dry density 1,580 kg/m^3.*

Appendix 2

Determination of basic geotechnical properties

The base variables water content w, void ratio e and degree of saturation S_r were determined according to Equations A2-1 to A2-3.

$$w = \frac{m_{tot} - m_s}{m_s} \quad \text{(A2-1)}$$

$$e = \frac{\rho_s}{\rho}(1 + w) - 1 \quad \text{(A2-2)}$$

$$S_r = \frac{\rho_s \cdot w}{\rho_w \cdot e} \quad \text{(A2-3)}$$

where

m_{tot} = total mass of the specimen

m_s = dry mass of the specimen

ρ_s = particle density

ρ_w = density of water

ρ = bulk density of the specimen

The dry mass of the specimen was obtained from drying the wet specimen at 105°C for 24h. The bulk density was calculated from the total mass of the specimen and the volume determined by weighing the specimen above and submerged into paraffin oil.

For determination of void ratio and degree of saturation the particle density ρ_s = 2,780 kg/m^3 and water density ρ_w = 1,000 kg/m^3 were used.